Astronuclear
WANL-TNR-102
APRIL, 1963

SUBMITTED BY:

Westinghouse Electric Corporation
Astronuclear Laboratory
Pittsburgh 36, Pennsylvania

AUTHORS.

F.A. Campi

J.W.H. CHI

E.A. DeZubay

J.D. Holmgren

A.M. Vetere

TRANSIENT TWO-PHASE HEAT TRANSFER AND FLOW CHARACTERISTICS OF LIQUID HYDROGEN

TABLE OF CONTENTS

TABLE OF CONTENTS

(Continued)

TABLE OF CONTENTS
(Continued)

LIST OF TABLES

TABLE OF CONTENTS
(Continued)

LIST OF FIGURES

TABLE OF CONTENTS

(Continued)

LIST OF FIGURES

TABLE OF CONTENTS

(Continued)

LIST OF FIGURES

SUMMARY

This report summarizes the initial phase of a program designed to evaluate transient two-phase heat transfer and flow characteristics of hydrogen as an integral part of the NERVA reactor requirement. To carry out these studies, a hydrogen facility and cryogenic laboratory was built and experiments were performed to obtain the desired data.

The experimental program included studies of single phase heat transfer, two-phase flow, and forced convection transient boiling heat transfer. The investigations were made with cold gaseous and liquid hydrogen flowing through horizontal test sections over the following range of conditions; inlet pressure 15 to 45 pounds per square inch absolute, flow rate 0.001 to 0.005 pounds per second, and temperature differentials of 10 to 500°R between the fluid and the wall. Two different test sections were used: a thin-walled copper tube (3/16" I.D. x 1/4" O.D.) and a heavier walled aluminum tube (3/16" I.D. x 1" O.D.).

Cool-down temperature, cool-down time, single phase heat transfer coefficients, transient two-phase flow characteristics and two-phase heat transfer coefficients are presented. Based on the transient fluid temperature data obtained, it has been shown that in the film boiling and transitional regimes, the thermodynamic equilibrium cannot exist between the vapor and the liquid. The mechanisms of two-phase flow during cool-down has been discussed in detail and a two-phase flow model has been postulated. The model provides a simple method for the determination of vapor fractions from temperature traces; a knowledge of the vapor fractions is a prerequisite for the understanding and prediction of two-phase heat transfer.

TRANSIENT FLOW EXPERIMENTAL RESULTS

1.0 INTRODUCTION

The experimental results discussed in this report arise from the flow problems associated with the initial start-up and subsequent restart requirements of the NERVA reactor. In the flow path of the hydrogen between the tank and the exhaust of the nozzle, the liquid hydrogen must in succession pass through the shut-off valve, the turbine, the cooling passage of the nozzle, the reflector, shield and reactor core, and finally exit through the nozzle. The behavior of the hydrogen flow at pressures below critical where two-phase conditions can exist is of vital importance during the start-up period. The part of the flow passage where the greatest change in the state conditions of the liquid hydrogen occur were in the reflector and control drums. In this region, small flow passage extend through a region of high thermal capacity associated with the reflector. The flow passage prior to the region, namely the piping and pump, have a relatively low thermal capacity so that the cool-down of these parts will occur rapidly while the cool-down of the reflector will occur more slowly. The physical behavior of the reflector is essentially one of cooling a relative large mass of metal with a fluid stream containing both gaseous and liquid phases. During this investigation the general test philosophy of using the simplest geometry possible in the test section was followed. Liquid hydrogen was to be introduced to the entrance of a simple circular tube suitably instrumented. With such a general configuration, the fundamental phenomenon involved in the boiling of liquid hydrogen in tubes of small diameters could be investigated, devoid of complicating geometric factors. The entire experimental program was built around the concept that the simplest flow system would be used until such time as a complete understanding of the flow behavior and heat transfer was obtained. In addition, the cool-down of the metal would be investigated without and finally with power input in the form of resistance heating at rates capable of simulating the power dissipation in an actual nuclear reflector. The descriptions of

the facilities and test equipment used to obtain these behavior patterns is covered in the next subject.

2.0 DESCRIPTION OF TEST EQUIPMENT

2.1 FACILITY

The facility in which the hydrogen work, both liquid and gaseous was conducted, consists of two test cells having a floor space of 15' x 20' and each cell containing three reinforced concrete walls. The roof and the fourth wall are expandable and constructed from light-weight material. The control room is an adjacent structure separated from the test cells by an air space of 8". The test cell walls are constructed of heavy reinforced, high density concrete capable of withstanding an over pressure of 50 psi. Two windows in the back wall are made of bullet-proof glass capable of withstanding 150 psi over pressure. The fourth wall is a hinged structure made of wood and aluminum and covered with a 6 mil polyethylene translucent sheet. The polyethylene sheet will fail at the slightest pressure and vent this wall. The roof structure is made of fiberglas panels sealed against the wind with mastic cement. These panels will relieve at pressures of approximately one pound per square foot. A mesh steel shrapnel net covers the roof to catch the roof panels if they are lifted by a deflagration wave. The control room is a separate cinder block sturcture having windows in line with the bullet-proof test cell windows. All electric and hydraulic connections from the control room to the test cell are offset such that no inline opening exists. Adjacent to the control room, a large room houses the 3 megawatt D. C. power supply. The interior of the hydrogen test facility is shown on Figure 1.

2.2 TEST LOOP

The test loop, shown schematically on Figure 2 and in the photo on Figure 3, contains all the components necessary for the experimental investigation of the flow behavior. The liquid hydrogen is stored in one of four (super-insulated) dewars having a capacity of 175 liters. These dewars are used as both transport and operating containers. The piping carrying the liquid hydrogen is completely vacuum-jacketted from the dewar to the test section. Included in this part of the flow loop are gas purge lines and suitable bypass valves. The test section is mounted horizontally in a vacuum chamber, two sides of which are made of plexiglas. Downstream of the test section the piping is not vacuum-jacketted. This section of the piping contains the exit throttle valve, an orifice meter, and the exhaust hose to the vent stack, which discharges to the atmosphere 30 feet above the top of the test cell. Provisions are also made in the exhaust line to incorporate a suitable heater upstream of the orifice meter so that evaporation of any remaining liquid can be assured.

2.3 TEST SECTION

A sketch of the horizontal test sections utilized in this program is shown in Figure 4. Two test sections were used: the first was a 26-inch copper tube of 1/4" O.D. and 3/16" I.D. The copper test section was preceded by a vacuum-jacketted connector approximately 10 inches long and a glass section approximately 5 inches long. This configuration is shown on the lower part of Figure 3. The configuration of the aluminum test section was altered in order to reduce the thermal capacity of the test loop between the source of liquid hydrogen and the inlet of the test section. For these tests, the 10-inch vacuum jacketted connector was removed and the glass section was installed after the test section.

The test section and auxiliary components are structurally supported by a series of spiders and rods as shown in Figure 3. The end flange spiders have been machined to provide minimum support area in order to reduce heat leakage.

2.4 INSTRUMENTATION

The test loop and test section were instrumented with various mass flow, temperature and pressure measuring devices and the outputs were continuously recorded on a high speed Minneapolis-Honeywell recording oscillograph (Visicorder^{R}). Process fluid flow and pressure level were controlled by remotely operated valves upstream and downstream of the test section. Semi-automatic operation of the test loop was achieved by programming through a console control system.

The mass flow rates of hydrogen were calculated from the pressure drop across a standard sharp-edged orifice located downstream from the flow control valve. During the initial tests, calculated flow rates were checked by pressure-time data from the hydrogen gas cylinders. Close agreements were obtained between the observed flow rates and the orifice calculated values.

In the early phase of the test program, a Potter Instrument turbine type flow meter was evaluated as a means of measuring hydrogen mass flow rates. The sensing element was placed in the vacuum-jacketted portion of the test loop preceding the test section. Mass flow rates are based on a volume measurement of a fluid of known density. The results obtained with the Potter meter were unsatisfactory as a result of two-phase hydrogen flow. Under these conditions, the fluid density varied considerably and the meter provided inconsistent results.

Hydrogen and test section temperatures were measured by copper-constantan thermocouples which were installed on the outside wall and in the center of the 3/16" I.D. test sections. The thermocouples determined wall and stream temperatures at the inlet, mid length, and exit portions of the test section. In addition, hydrogen

temperatures at the orifice meter were measured for the purpose of calculating hydrogen mass flow rates and to assure that only single phase gaseous flow persisted through the orifice meter. Temperatures were continuously recorded with the Visicorder[R] at a normal chart speed of four inches per second. Transient behavior was easily discerned and recorded at this chart speed.

In order to obtain rapid thermocouple response time, a minimum-sized thermocouple bead was made using B & S 36 gauge wire (0.005 inch O.D.). For wall temperatures, the thermocouples were cemented directly to the tube. For stream temperatures, Teflon[R] insulated thermocouples were inserted through sheath-type assemblies which were soldered or cemented to the test section. In these instances, the bare couple junctions were positioned at the center of the test section.

The pressure drops across the test section and orifice meter were measured through a series of pressure taps connected to strain-gauge type transducers. Pressure values were also recorded continuously by the Visicorder[R]. The transducers were calibrated directly in the test loop using known pressure values and then checked against instrument outputs by utilizing calibration resistors which were installed in the amplifier circuit.

3.0 EXPERIMENTAL PROGRAM

3.1 PROCEDURE

The experimental tests were made by using a fixed operating procedure. Essentially, the prerun procedure consisted of (1) evacuating the cryogenic loop piping and test section vacuum chamber, (2) flushing the loop piping and test section with ambient temperature nitrogen followed by hydrogen, (3) precooling the loop piping with gaseous hydrogen at liquid nitrogen temperature, and finally (4) cool-down of the loop piping with liquid hydrogen. The test section was isolated from the test loop system following the ambient temperature hydrogen purge in order to maintain the test section at ambient temperature. A test was initiated by directing the liquid hydrogen flow through the test section after

the loop piping cool-down period. The vacuum chamber around the test section was pumped continuously during the test.

During a run, pressures and temperatures were continuously recorded on the high speed Visicorder[R]. In addition, the glass portion of the test section was monitored both visually and with a camera. Various low and high speed motion pictures were made in an effort to help evaluate and interpret the recorded data. The hydrogen flow rates varied from .001 to .005 pounds per second and the inlet pressure ranged from 15 to 45 pounds per square inch gauge.

3.2 TESTS

The initial shakedown tests on the cryogenic flow loop were completed with liquid nitrogen. The purpose of these tests was to check the loop for heat leak, evaluate the response time of the instrumentation and obtain preliminary cool-down rates. Subsequent tests were carried out with cold gaseous hydrogen and liquid hydrogen to check and evaluate the characteristics of the test apparatus. When using cold gaseous hydrogen, the specific interests were heat transfer coefficients, flow rates, and pressure drop measurements across the test section. Following this evaluation, tests were completed with liquid hydrogen to study forced convection transient boiling heat transfer.

The first test section studied was the thin-walled copper tube. The tube was used as a calorimeter and was selected to obtain the minimum response time for the evaluation of instrumentation as well as to minimize radial temperature gradients. When the nitrogen and hydrogen tests were completed on the copper test section, the flow loop was modified to reduce the thermal capacity of the flow system between the source of the liquid hydrogen and the inlet of the test section. The second test section was made of aluminum. It was fabricated to simulate the thermal capacity per unit heat transfer area of the beryllium reflector.

A preliminary analysis of the data obtained from the cold flow tests has been made. Based on this information, cool-down temperature histories, transient two-phase flow and heat transfer have been evaluated. The results from these studies are discussed in the following sections.

4.0 RESULTS

4.1 TEST SECTION COOL-DOWN

The analytical approach to the problem consisted of cool-down temperature histories calculated on closed form analytic solutions to simplified single step or lumped parameter equations (see Appendix I - 1.1 "The Lumped Parameter Model") as well as computer solutions using many step increments and sophisticated machine logic. In all cases the coolant was assumed to be liquid hydrogen entering the tube at time zero. The histories of these single step solutions are shown on Figure 5 for materials of copper, aluminum and beryllium. It will be noted that time constants of 0.6 seconds for copper and 0.4 seconds for aluminum and beryllium are obtained. Using this time constant (time required for the temperature difference to attain e^{-1} of the initial and final temperature difference) as a measure of the cool-down time (Appendix I, 1.2 "Time Constant Definition"), the analytic and experimental results with the copper test section can be compared on Figure 6.

The single step solution was modified to account for the time delay resulting from the concentration of the metal at one half the tube length; that is, the coolant flows through a tube with no thermal effects for one half its length where a lump representing all of the thermal properties of the actual tube is concentrated. The temperature used to determine the time constant for the computer solution was the axial midpoint temperature of the tube. The "measured" curve used the data from the experiments modified for the delay of the liquid hydrogen in reaching the test section. The comparisons of the time constants show that the measured values of the time constants are approximately four

times higher than those calculated. This suggests that the heat transfer coefficients under the transient conditions of our experiments were materially lower than the values used in the calculations, which had been obtained under steady-state conditions. A detailed discussion on two-phase heat transfer will be presented in a later section.

In order to simulate the conditions existing in the reactor, the flow loop was modified to reduce the thermal capacity of the flow system and the copper test section was replaced with the aluminum unit. The data obtained from the heavier-walled aluminum section is in good agreement with that obtained from the copper test section. Comparisons of the calculated and experimental cool-down times indicated the same order of magnitude of discrepancies observed previously with the copper section. The measured cool-down times for the aluminum tube are three to five times those calculated. The cool-down times as a function of the mass flow are shown on Figure 7. It should be noted that good agreement was obtained between the results of these tests when compared to those obtained from data reported by Los Alamos Scientific Laboratory.

4.2 HYDROGEN FLOW AND HEAT TRANSFER CHARACTERISTICS

The cold gaseous hydrogen test runs were performed to: (1) check the heat transfer equation for correlating single phase local heat transfer coefficients, and (2) determine the accuracy of the pressure drop measurements across the test section. The copper test section was used for these tests. Hydrogen gas was obtained from a series of manifolded tanks and was cooled to near liquid nitrogen temperature prior to entering the test section.

The inlet and outlet wall and fluid temperature histories for a typical run, 1-GH-1, are shown in Figure 8. The static pressure and pressure drop histories for the same run are plotted in Figure 9. As seen from these figures, the pressure in the system reached steady-state within a few seconds; however, the temperatures did not achieve steady-state values until thirty seconds or more.

4.2.1 HEAT TRANSFER COEFFICIENTS

Neglecting axial conduction and radial temperature differences in the tube, a shell energy balance on a differential section of the tube of length ΔL gives

$$- h \pi D_i \Delta L (T_w - T_f) = - \rho C_p \frac{\pi}{4} (D_o^2 - D_i^2) \Delta L \frac{d T_w}{d t}$$

or

$$h = - \rho \frac{C_p (D_o^2 - D_i^2)}{4 (T_w - T_f) D_i} \frac{d T_w}{d t} \qquad (1)$$

Equation 1 is independent of position; hence it defines the local heat transfer coefficient at any point along the tube. The calculation of the local heat transfer coefficient should be based on the inside wall temperature; however, the combination of a high thermal conductivity for copper and the thin wall of the tubing resulted in a negligible temperature difference across the wall so that the outside wall temperatures can be used. An estimate of the temperature difference across the tube under experimental conditions indicated that it was of the order of $0.5^{\circ}R$. At any given time the slope $\frac{d T_w}{d t}$ was determined by graphical differentiation of the time-wall temperature curve. Cryogenic properties of copper were obtained from Reference 1.

Based on a recent literature survey[2], the recommended equation for correlating single phase local heat transfer coefficients for hydrogen is:

$$N_{Nu} = A\,(N_{Re})^{.8}\;(N_{Pr})^{.4}\;\left(\frac{T_w}{T_f}\right)^{-B}\left[1 + C\left(\frac{X}{D_i}\right)^{-D}\right]$$

Where X is the distance from the entrance to the test section, and A, B, C, and D are constants. The recommended values are:

$$A = .025$$

$$B = .55$$

$$C = .3$$

$$D = .7$$

A short section (5 3/4") of glass tubing preceded the point at which inlet measurements were made, and the location at which exit measurements were made is 24 inches down-

stream from the inlet plane; therefore, $\frac{X}{D}$ is very large and the term $1 + C\left(\frac{X}{D_i}\right)^{-D}$ becomes 1. Under the experimental conditions, the ratio $\frac{T_w}{T_f}$ was always less than 2. For $\frac{T_w}{T_f}$ less than 2, McCarthy and Wolf[3] recommended the coefficient A to be .023. Accordingly, the equation used for predicting local heat transfer coefficients is

$$\frac{h D_i}{K} = .023 \left(\frac{4 W}{\pi D_i \mu_L}\right)^{.8} \left(\frac{C_p \mu}{K}\right)^{.4} \left(\frac{T_w}{T_f}\right)^{-.55} \qquad (2)$$

The local heat transfer coefficients calculated and predicted by Equations 1 and 2, respectively, are compared in Table I.

TABLE I

COMPARISON OF EXPERIMENTAL AND PREDICTED LOCAL HEAT TRANSFER COEFFICIENTS

($h \times 10^3$ BTU/in.^{2}-sec. - $^\circ$R)

t, Seconds	T_f $^\circ$R	Based on Tube Inlet Data		Based on Tube Exit Data	
		Experimental Equation (1)	Predicted Equation (2)	Experimental Equation (1)	Predicted Equation (2)
		Run 1-GH-1 $\bar{w}$ = .00208 lb./sec.			
5	358	.66	.80	.89	.84
6	352	.61	.80	.78	.83
7	343	.62	.79	.71	.83
8	342	.57	.79	.81	.82
9	340	.57	.79	.72	.82
10	339	.51	.78	.82	.81
		Run 1-GH-2 $\bar{w}$ = .00298 lb./sec.			
6	322	.54	1.01	1.26	1.06
8	310	.42	1.00	1.38	1.02
10	305	.37	.98	1.58	1.01
12	296	.37	.96	1.37	.99
14	287	.32	.96	1.53	.99

$h \times 10^3$ BTU/in.^{2}-sec. - $^\circ$R

Run	Average Observed	Predicted	% Deviation
1-GH-1	.69	.80	16
1-GH-2	.92	1.00	8.7

Within the range of temperatures encountered in a given run, the predicted local heat transfer coefficients were practically constant. At the inlet plane of the test section, the predicted heat transfer coefficients were consistently higher than those determined experimentally whereas at the exit of the test section, the experimental values were equal to or greater than those predicted. The observed deviations were reduced and an improved correlation of the data was obtained when the value of Constant A (Equation 2) was changed from 0.023 to 0.0205. Values of A as low as 0.0196 have been reported in the literature. It should be noted that a variety of exponents for the temperature ratio, Reynold's, and Prandtl's numbers have been used by previous investigators. In view of these divergencies, the agreement between observed and predicted heat transfer coefficients is quite good.

4.2.2 PRESSURE DROP

Neglecting kinetic energy changes, the pressure drop across the test section can be calculated from the standard equation

$$\Delta P = \frac{2 f L \rho V^2}{D_i g_c} \qquad (3)$$

where f is the friction factor, L is the length of the tube over which the pressure drop is measured, and V is the average fluid velocity.

The fanning friction factors used in Equation (3) were obtained from Reference 4. The approximate steady-state fluid temperature of 280°R for Run 1-GH-1 and 250°R for Run 1-GH-2 were used to determine the fluid properties. The observed and predicted pressure drops are compared in Table II.

Table II

COMPARISON OF PRESSURE DROPS

Pressure Drop, PSI

Run	Observed	Predicted	Per Cent Deviation
1-GH-1	4.6	3.7	- 19.5
1-GH-2	6.4	5.8	- 9.4

The agreement between predicted and observed pressure drops are fairly good, considering that errors in measuring flow rates as well as flow disturbances due to thermocouples and other unknown geometric factors have not been taken into account.

4.2.3 COMPARISON OF EXPERIMENTAL AND COMPUTED DATA

Based on equations of continuity, motion, and energy a computer program was written by the Reactor Analysis group for the transient fluid flow and heat transfer in the NERVA reactor. The program is readily adaptable to single phase flow and heat transfer calculations. With the same initial conditions as those found in

experimental Run 1-GH-1, the temperature and pressure drop histories for the test section were computed. The results for the exit plane of the test section are compared with the measured values in Figure 10. At the inlet to the test section, the maximum deviation in wall temperature is 3% and that of the fluid is 1%; the average deviations are negligible. This close agreement is expected since the pressure and flowrate inputs to the computer as well as the initial temperatures were based on the experimental data.

The more significant comparisons are those at the exit of the test section. As seen from Figure 10, the computed temperatures at the exit to the test section are in general lower than the measured values. The average deviation in wall temperatures is 2% with a maximum of 5%. The average deviation in fluid temperatures is 2% with a maximum of 6%. The deviations are well within the experimental error.

A comparison of measured and computed pressure drops is shown in Figure 11. As seen from the Figure, the measured pressure drops are consistently higher than those computed. This is readily explained by the fact that thermocouples had been inserted into the stream for the measurement of fluid temperatures, resulting in additional friction; consequently, higher pressure drops were observed. The apparent "equivalent roughness factor" for the test section is 1.5 (compared to a smooth tube). The hand-calculated, steady-state pressure drop based on a "rough" pipe is seen in Figure 11 to be between the computer calculated values for a smooth tube and those observed experimentally.

4.3 TRANSIENT TWO-PHASE FLOW

In order to better understand two-phase flow and boiling heat transfer to hydrogen at transient conditions, the mechanisms of two-phase flow in the film boiling, transitional and nucleate boiling regimes were investigated. Based on the hydrogen

temperature data obtained from the cool-down studies, a two-phase flow model was postulated. The model provides a simple method for the determination of vapor fractions from temperature traces. The vapor fractions determined have been verified by values calculated from an independent procedure.

A typical schematic inlet stream temperature history covering the unsteady-state period of interest is shown in Figure 12. The temperatures were recorded on a Visicorder® at a chart speed of 4 inches per second. Since the test period of interest was generally 20 seconds or more in duration, much of the significance of the temperature fluctuations observed is lost on the time scale used in Figure 12; therefore, blow-ups of the temperature traces for typical time increments are reproduced in Figure 13.

Following Figure 12, it is evident that the temperature-time trace is initially very smooth, but fluctuates with time thereafter. A few seconds after the admission of fluid into the test section, saturation temperature appeared fleetingly. With increasing time, the saturation temperature, i.e., liquid, appeared more frequently and persisted for longer periods. This can be readily seen from the sequence of blow-ups shown in Figure 13. Based on these results, the following mechanisms appeared to occur during cool-down.

4.3.1 MECHANISMS OF TWO-PHASE FLOW

Initially, due to the large temperature difference between the wall and the saturated liquid, any liquid admitted to the test section is flashed-off to vapor. As the wall temperature or heat transfer decreases, there is insufficient sensible heat within the vapor to boil off all the liquid admitted, resulting in dispersed or "spray"

flow. Gradually, the dispersed liquid droplets agglomerate to form slug flow. As seen from Figure 13, the sudden changes in temperature from vapor to liquid suggest the appearance of alternate slugs of vapor and liquid. The successive heat transfer regimes are: heat transfer to a vapor, film boiling, transitional boiling, and nucleate boiling. A schematic diagram showing the idealized modes of two-phase flow is shown in Figure 14. The sequence of two-phase flows described above is in general agreement with those observed visually by Bronson, et.al.[5]

In the film boiling regime, the vapor is in equilibrium with the liquid only at the vapor-liquid interface. Everywhere else the vapor is superheated. Due to the unsteady nature of heat transfer and the relatively poor conductivity of the vapor, thermodynamic equilibrium cannot be attained; therefore, the mass fraction vapor at any instant is not equivalent to the thermodynamic quality.

4.3.2 VAPOR FRACTIONS

Under the conditions of the experiments, the two-phase flow through the test section is highly turbulent; therefore, in mist flow it can be assumed that the two-phase fluid exists as a homogenous mixture with the vapor at an average temperature T_v and the liquid at its saturation temperature, T_{sat}. This implies that the liquid droplets are in random motion.

Consider the thermocouple bead as the control volume. In mist flow, if the droplets of liquid are equal to or smaller than the control volume, then the appearances of the saturation temperature are instantaneous. If the liquid droplets or slugs are large relative to the control volume, then the saturation temperature appears for a finite time.

The cumulative liquid residence time, t_L was determined from the Visicorder^R tape and it can be plotted versus the total time, t. A typical curve of t_L vs t is shown in Figure 15. It is evident from the large amount of existing data that in the absence of

sudden external disturbances, such as pressure surges and heat leaks, the cumulative liquid residence time can be treated as a continuous and single-valued function of time.

The void fraction at any time can be obtain from the slope of the t_L vs t curve, (see Appendix II, 1.4). The void fractions for two typical experiments at different flowrates are presented in Figure 16 as a function of total time. The instantaneous local vapor fractions at the inlet to the test section were calculated on the assumption that the void fraction is proportional to the fraction of the time vapor temperatures were observed. Due to the fact that heat was transferred to the fluid along the length of the test section, the liquid was vaporized continuously down the test section, and the corresponding slug flow phenomenon at the exit to the test section was not observed until a much later period. By this time, the test section had cooled down considerably so that the temperature fluctuations (between vapor and liquid) were less pronounced and liquid residence time could not be determined as readily. Nevertheless, based on the vapor fractions calculated for the inlet to the test section, those at the outlet can be computed from energy balances around the test section (Appendix II, 1.6). The calculated vapor fractions for two typical runs are shown in Figures 17 and 18.

The average vapor fractions over the entire test section were estimated from the average two-phase fluid velocities (Appendix II, 1.7). Typical results are compared with the inlet and exit instantaneous vapor fractions in Figures 17 and 18. The average of the local values were calculated and plotted versus those estimated from fluid velocities in Figure 19. As seen from this Figure, the vapor fractions determined by the two methods are in good agreement. The values estimated from velocities were on the average 10% lower than those computed from the two-phase flow model.

4.3.3 DISCUSSION

The most important conclusion resulting from this work is that thermodynamic equilibrium between the vapor and liquid phases does not exist in the film boiling and transitional regimes during cool-down. In fact, superheated vapor was found to exist simultaneously with the saturated liquid.

Previous investigators[6,7] on two-phase flows and boiling heat transfer to hydrogen in steady-state systems have not measured stream temperatures but assumed that the vapor and liquid are in equilibrium. On this basis, the vapor fractions or qualities were determined with the aid of thermodynamic properties and energy balances. It becomes obvious that the application of the same assumption to the unsteady-state system studied here can introduce serious errors in the vapor fractions determined.

4.4 TWO-PHASE HEAT TRANSFER

As discussed in Section 4.2, the local heat transfer coefficient can be calculated from the equation

$$h = - \frac{\rho C_p \delta \, d T_w/dt}{T_{Wi} - T_f} = \frac{Q/A}{T_{Wi} - T_f} \qquad (1)$$

where T_f is the fluid temperature. In the case of a single phase flow, T_f is readily defined as the bulk fluid temperature; however, in non-equilibrium two-phase flow, it has been shown that the fluid temperature oscillates between that of the vapor and the liquid. From the above equation, it becomes apparent that, depending on the fluid temperature chosen, a variety of two-phase heat transfer coefficients can be calculated.

In order to determine a significant definition of T_f, it is necessary to examine closely the mechanisms of two-phase flow.

Hendricks[7], et.al., Wright and Walters[6], and Ellerbrock[8], et.al. studied boiling heat transfer of hydrogen under steady-state as well as transient conditions. These investigators assumed saturation temperatures for the fluid at all positions along the heated test section for all times. In the system studied here, superheated vapor temperatures as well as the saturation temperature were measured intermittently. This fact precludes the assumption of saturation temperatures for the fluid. From a detailed analysis of the fluid temperature traces observed, it has been concluded in a previous section that slug flow phenomenon predominates during cool-down. It is evident that with slug flow, the tube wall at any location is alternately in contact with either all vapor or a thin film of vapor with a liquid core (in the film boiling regime). Assuming that the vapor film is negligible, then the slug flow phenomenon suggests a time-averaged bulk fluid temperature. In terms of the relative times of observing the vapor and liquid, or the void fraction, the indicated fluid temperature is:

$$\bar{T}_f = \epsilon\, T_v + (1 - \epsilon)\, T_{sat} \qquad (4)$$

and

$$T_w - T_f = \epsilon\, (T_w - \bar{T}_v) + (1 - \epsilon)\, (T_w - T_{sat})$$

or

$$T_w - T_f = (T_w - T_{sat}) - \epsilon\, (\bar{T}_v - T_{sat}) \qquad (5)$$

A two-phase heat transfer coefficient can now be defined by the equation

$$-\frac{\rho C_p \delta \, d T_w}{d t} = h_{TP}\left[\left(T_w - T_{sat}\right) - \epsilon\left(\bar{T}_v - T_L\right)\right] \qquad (6)$$

On the time-fluid temperature trace, a smooth curve was drawn through the maximum observed fluid temperatures to determine the average vapor temperatures. The range of temperatures observed between those of the vapor and that of the liquid are assumed to be due to the finite response time of the thermocouples.

Figure 20 shows some typical wall temperature histories of the copper and aluminum test sections during cool-down. For the thick-walled aluminum tube, the wall temperatures measured at three radial positions at the same plane are plotted together. In the aluminum tube, the radial temperature gradients are within the accuracy of the wall temperature measurements ($\pm 8^{\circ}$). The slopes $d T_w/d t$, to be used in the calculation of the heat transfer coefficient were determined by graphical differentiation of a smooth curve drawn through the wall temperature-time traces.

4.4.1 TWO-PHASE HEAT TRANSFER COEFFICIENTS

It is generally known that for a given fluid at a constant pressure, a plot of either heat flux or the two-phase heat transfer coefficient versus the temperature difference describes a unique curve characterized by a maximum heat flux for nucleate boiling and a minimum for film boiling. From the wall and fluid temperature histories measured during cool-down, the two-phase heat transfer coefficients were calculated by Equation 6. The corresponding heat transfer coefficients in the film boiling regime are shown in Figure 21 for both the copper and aluminum test sections. Below a temperature difference of 10°F (in the transitional and nucleate boiling regimes), small errors in the measured

temperatures can cause large errors in calculated heat transfer coefficients; hence the heat transfer coefficients in these regimes could not be determined accurately.

From a comparison of the heat transfer coefficients determined from the two test sections it is evident that the values calculated from the aluminum tube are, in general, lower than those calculated for the copper tube. The data obtained in this investigation are compared to information found in the literature, as shown in Figure 22. The ranges of variables investigated are compared in Table III. The data of Wright and Walters[6] and Hendricks, et.al.[7] represent average values and it is apparent that all the data are in fair agreement. The scatter of the data are within the experimental accuracy anticipated in this type of data since it is known that in a plot of h versus ΔT, the correlation is very sensitive to pressure. As seen from Table III, the data were taken over a range of pressures which may account for some of the scatter in the data.

4.4.2 TWO-PHASE HEAT TRANSFER MODEL FOR THE FILM BOILING REGIME

The detailed mechanisms of two-phase flow during cool-down have been discussed. Based on the mechanisms in the film boiling regime, the following physical models for two-phase heat transfer are postulated. It is assumed that in mist flow and slug flow, the liquid and vapor form discrete plugs. The plugs of liquid are assumed to be relatively small in mist flow. The time interval between plugs is determined by the void fraction. On the basis of this model, it appears that the total heat transferred to the two-phase fluid can be taken as the sum of the fraction of heat transferred to single phase vapor and the fraction of heat transferred to liquid plugs. In the film boiling regime, the liquid plugs are surrounded by a vapor film.

TABLE III

COMPARISON OF EXPERIMENTAL CONDITIONS FOR FORCED CONVECTION BOILING HEAT TRANSFER TO HYDROGEN IN A SINGLE TUBE

Data Source	TEST SECTION				Mass Flowrate lb./sec.	Pressure Psia
	Material	Diameter, Inches		Position		
		Inside	Outside			
WADC TR-59-423	Copper	1/4	3/4	Horizontal	.290 to .826	24 to 32.8
NASA TN-D-765	Inconel	.344	3/8	Vertical	.063 to .181	27.0 to 70.2
WANL	Copper	3/16	1/4	Horizontal	.0012 to .0033	14.7 to 36.7
WANL	Aluminum	3/16	1	Horizontal	.0011 to .0048	14.7 to 45.7

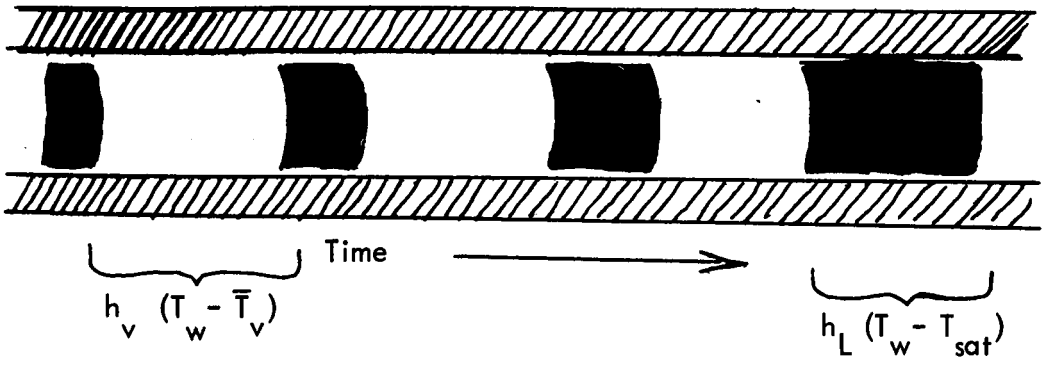

HEAT TRANSFER MODEL
FOR THE FILM BOILING REGIME

Mathematically, the model can be represented by a general equation for two-phase heat transfer:

$$-\rho C_p \delta \frac{d T_w}{d t} = \epsilon h_v (T_w - T_v) + (1 - \epsilon) h_L (T_w - T_L) \qquad (7)$$

in which

ϵ = The void fraction (See Appendix 1.5)

h_v = Local vapor heat transfer coefficient, calculated from Equation 2

In the above equation, h_L is defined as the local heat transfer coefficient for heat transfer to liquid plugs. Equations 6 and 7 can be combined to give

$$h_{TP} \left[(T_w - T_L) - \epsilon (\bar{T}_v - T_L)\right] = \epsilon h_v (T_w - \bar{T}_v) + (1 - \epsilon) h_L (T_w - T_L) \qquad (8)$$

4.4.3 MECHANISMS OF TWO-PHASE HEAT TRANSFER

It is postulated that heat is transferred by a two step mechanism: First, heat is transferred from the wall to the fluid, which is then transferred from the vapor to the liquid. The fluid referred to here is the time-averaged bulk material flowing past any point at any time. Let $Q_{w \rightarrow f}$ denote the instantaneous heat transfer from the wall to the fluid. It is evident that for an incremental volume of the test section, ΔV,

$$Q_{w \rightarrow f} = -\rho C_p \Delta V \frac{d T_w}{d t} \qquad (9)$$

The existence of two-phase flow during transient cool-down implies the following possible situations:

1. The rate of heat transfer from the wall to the fluid at any instant is less than the rate of heat transfer from the vapor to the liquid, i.e., heat transfer from the wall to the fluid is rate controlling. Mathematically, this is expressed as:

$$Q_{w \rightarrow f} < Q_{v \rightarrow L} \qquad (10)$$

2. The instantaneous rate of heat transfer from the wall to the fluid equals the instantaneous rate of heat transfer from the vapor to the liquid, but is less than that required to vaporize the remaining liquid:

$$Q_{w \rightarrow f} = Q_{v \rightarrow L} < (1 - y) \lambda W \qquad (11)$$

3. The transfer of heat from the wall to the fluid is rate controlling, but the rate of the heat transfer is less than that required to vaporize all the liquid:

$$\lambda W (1 - y) > Q_{w \to v} < Q_{v \to L} \qquad (12)$$

It follows that if the instantaneous rate of heat transfer from the vapor to the liquid is greater than that required to vaporize all the liquid $\left[Q_{v \to L} > \lambda W (1 - y)\right]$, then single phase vapor results. This is the situation observed at the initiation of cool-down. Under these conditions, $\epsilon = 1$ or $\epsilon \approx 1$, and Equation 8 reduces to

$$h_{TP} = h_v \qquad (13)$$

and the energy balance becomes

$$-\rho C_p \delta \frac{d T_w}{d t} = h_v (T_w - \bar{T}_v) \qquad (14)$$

In the slug flow regime, it has been observed that if the liquid plugs are relatively far apart, the average vapor temperature may approach the wall temperature, and $T_w - \bar{T}_v$ is negligible compared to $T_w - T_L$.

Equation 8 then reduces to

$$h_{TP} = h_L \qquad (15)$$

and

$$-\rho c_p \delta \frac{dT_w}{dt} = (1 - \epsilon)\, h_L (T_w - T_L) \qquad (16)$$

4.4.4 PREDICTION OF TWO-PHASE HEAT TRANSFER

For two-phase flow where $\epsilon \geq .95$, the heat transfer data have been correlated by Equation 13 . The following table is a comparison of experimental and predicted heat transfer coefficients at two mass flowrates. The h_v's have been calculated from the modified Dittus Boelter Equation 2.

TABLE IV
COMPARISON OF OBSERVED AND PREDICTED HEAT TRANSFER COEFFICIENTS

$\bar{w} \times 10^3$ lb./sec.	t, Time from Initiation of Cool-Down, Seconds	ϵ, Volume Fraction Vapor (Void Fraction)	y, Mass Fraction Vapor	$h_v \times 10^3$, Calc. Btu/in^2-sec-$^\circ$R	$h_{TP} \times 10^3$, Obs. Btu/in^2-sec-$^\circ$R	% Deviat
3.3	1	.992	.208	.783	.615	- 11.0
	2	.982	.129	.877	.765	- 14.6
	3	.967	.093	.825	.896	+ 7.9
	4	.950	.065	.828	.970	+ 4.3
1.1	1	.995	.30	.522	.482	- 8.3
	2	.993	.247	.500	.610	+ 18.0
	4	.988	.175	.476	.530	+ 10.2
	6	.979	.120	.457	.450	- 1.6
	8	.967	.082	.443	.405	- 9.4
	10	.950	.060	.430	.392	- 9.7
						$\pm$ 8.5

As shown in the Table, the average deviation between observed and predicted heat transfer coefficients is $\pm$ 8.5%, which is better than that for single phase heat transfer (Section 4.2). This close check suggests that Equation 2 can be used with confidence to calculate heat transfer coefficients for the vapor phase in two-phase flow.

Analysis and correlation of heat transfer data in other flow regimes (where $\epsilon < .95$) are incomplete. A generalized correlation of h_L is being sought. It becomes apparent from the foregoing discussion that boiling heat transfer is exceedingly complex. In order to predict line cool-down and the modes of two-phase flow, the void fractions must be predicted.

4.4.5 STEADY-STATE TWO-PHASE HEAT TRANSFER

Wright and Walters[6] and Hendricks et.al.[7] have studied two-phase heat transfer to hydrogen under steady-state conditions Hendricks et.al. assumed an annular flow model with a liquid core. Based on this model, heat transfer coefficients were calculated from the relationship

$$\frac{Q}{A} = h_{TP}(T_w - T_L) \qquad (17)$$

It is apparent that this represents a special case of the general two-phase heat transfer Equation 6. In this case ϵ can be regarded as the fraction of the time single phase vapor flows past any given plane, which is 0. Hence Equation 6 becomes identical to Equation 17, since $\frac{Q}{A} = -\rho C_p \delta \frac{dT_w}{dt}$

4.4.6 DISCREPANCIES BETWEEN COMPUTER CALCULATED AND EXPERIMENTAL COOL-DOWN

In predicting cool-down, the transient start-up program requires the following assumptions:

1. The fluid enters the test section as a liquid with zero quality.
2. All the heat transferred to the fluid turns up as latent heat of vaporization until all the liquid is vaporized, i.e.

$$Q_{w \rightarrow f} = Q_{v \rightarrow L}$$

3. The fluid temperature is at the boiling point during two-phase flow; hence heat transfer is based on the assumption $Q/A = h_{TP} (T_w - T_L)$

From the discussions in the foregoing sections, it is apparent that assumption 1 is incompatible with the actual experimental conditions. However, this has been avoided by introducing experimentally determined quality and temperature versus time data at the entrance of the test section to the computer. The computer determined exit wall and stream temperatures as well as the qualities were then compared with the experimental data. The results have shown discrepancies in cool-down times of the same order of magnitude as given before. In addition, computed qualities were much higher than the experimental values; the former were nearly 1 at all periods of interest. These discrepancies can be expected from the requirements of assumptions 2 and 3.

5.0 CONCLUSIONS

Based on data obtained from the study of pressurized cool-down of selected test sections with cold gaseous and liquid hydrogen, it has been shown that:

1. Two-phase heat transfer predicted by the transient start-up program is much more efficient that that observed.

2. For single phase flow and heat transfer to gaseous hydrogen at cryogenic temperatures, the pressure drops and heat transfer behavior under transient conditions can be readily predicted from well established equations and generalized correlations determined from steady-state experiments.

3. In the film boiling and transitional regions, thermodynamic equilibrium does not exist between the vapor and the liquid. A superheated vapor was found to exist simultaneously with the liquid at its boiling point.

4. The vapor fractions can be determined from fluid temperature traces and they can be checked closely with values based on instantaneous velocities and mass flowrates.

5. Calculated two-phase heat transfer coefficients are in good agreement with data obtained by other investigators.

6.0 FUTURE WORK

The next phase of the Transient Flow Program will investigate various single and multiple pass test sections,heated and unheated, to be evaluated in the horizontal as well as the vertical positions. Test conditions of interest include liquid hydrogen from atmospheric to high pressures. Every effort will be made to simulate exact operating conditions.

In order to permit better comparisons of experimental data with those computed by the transient start-up program, it is necessary that the boundary conditions used by the computer be identical to those occurring under experimental conditions. Towards this end, two approaches are being taken to establish the same conditions at the inlet to the test section:

1. A three-way cryogenic valve will be installed preceding the entrance to the test section. This will reduce the thermal capacity in front of the test section so that an all liquid feed can be more nearly attained.

2. Quality meters and all available techniques for measuring qualities will be evaluated and tested in an effort to determine accurately the inlet and exit fluid conditions.

Simultaneously, attempts will be made to improve heat transfer by minimizing the superheat in the vapor. Various mechanical turbulence generators, baffles, etc. will be investigated in the hope of creating a greater vapor-liquid interfacial area for more efficient heat transfer.

Continued efforts will be made to correlate the heat transfer and fluid flow data in forms that can be readily utilized by a computer program. Moreover, two-phase flow models will be developed and refined in an attempt to provide a sound basis for predicting transient start-up of the NERVA engine.

REFERENCES

1. "A Compendium of the Properties of Materials at Low Temperature, Part II", WADC-TR-60-56, October, 1962.

2. Thomas, G. R., "An Interim Study of Single Phase Heat Transfer Correlations Using Hydrogen", WANL-TNR-056, April, 1962.

3. McCarthy, J. R., and Wolf, H., "The Heat Transfer Characteristics of Gaseous Hydrogen and Helium", RR-60-12, December, 1960.

4. McAdams, W. H., "Heat Transmission", McGraw-Hill Book Company, 3rd Edition, 1954, p. 156.

5. Bronson, J. C., et.al., "Problems in Cool-Down of Cryogenic Systems", Advances in Cryogenic Engineering, Volume 7, Plenum Press, New York, 1962, p. 201.

6. Wright, C. C., and Walters, H. H., "Single Tube Heat Transfer Tests, Gaseous and Liquid Hydrogen", WADC Technical Report 59-423, 1959.

7. Hendricks, R. C., et.al., "Experimental Heat Transfer and Pressure Drop of Liquid Hydrogen Flowing Through A Heated Tube", NASA-TN D-765, 1961.

8. Ellerbrock, H. H., et.al., "Fluid Flow & Heat Transfer Problems in Nuclear Rockets", to be published soon by NASA.

APPENDIX I

NOMENCLATURE

A	=	a constant
A'	=	a coefficient, a function of
B	=	a constant
C	=	a constant
C_o	=	orifice coefficient, a function of
C_p	=	heat capacity
D	=	tube diameter
D_a	=	upstream inside diameter for the orifice
D_i	=	inside diameter of the test section
D_o	=	outside diameter of the test section
F_{Re}	=	a viscosity correction factor
f	=	friction factor
g_c	=	a conversion factor, 32.2 $ft\text{-}lb_m/lb_f\text{-}sec^2$
h	=	local heat transfer coefficient
K	=	specific heat ratio of the fluid
k	=	thermal conductivity
L	=	length of the test section

N_{Re} = Reynold's number

N_{Pr} = Prandtl number

P = pressure

P_a = orifice upstream static pressure

P_b = orifice flange tap static pressure

$\overline{Q}$ = average heat transferred from the wall to the fluid

r = radius of test section

S = inside tube cross-sectional area

S_o = orifice cross-sectional area

t = time

t_L = cumulative liquid residence time

t_v = cumulative vapor residence time

Δt_L = a constant

T = temperature

T_f = fluid temperature

v = volume fraction

V = average fluid velocity

W = mass flow-rate

X = distance from inlet to the test section

y = mass fraction vapor

Y	=	expansion factor
a	=	proportionality constant
β	=	ratio of orifice diameter to upstream tube diameter
δ	=	$\frac{D_o^2 - D_i^2}{4D}$
λ	=	latent heat of vaporization
ρ	=	density of tube
ρ_a	=	orifice upstream fluid density
ρ_f	=	average fluid density in the test section
τ	=	lag time between temperature traces at the inlet and outlet of the test section
ϕ	=	angle

Subscripts:

f	=	fluid
i	=	inside
L	=	saturated liquid
o	=	outside or initial
TP	=	two-phase
v	=	vapor
w	=	wall
1	=	inlet
2	=	outlet

APPENDIX II

1.1 THE LUMPED PARAMETER MODEL

In order to evaluate the limitations of the lumped parameter model used as a comparison between measured and computer-determined cool-down results, its derivation will start with the generalized heat transfer equation so that the significance of the approximations becomes obvious. The generalized heat transfer equation for conduction in solids is usually written as

$$c_p \rho \frac{\partial T}{\partial t} = k \nabla^2 T \tag{18}$$

If this is applied to a solid rod or hollow tube using a three dimensional coordinate system in r, $\emptyset$, and $\not{z}$;

$$\nabla 2 = \frac{\partial^2}{\partial r^2} + \frac{1}{r^2} \frac{\partial^2}{\partial \emptyset^2} + \frac{1}{r} \frac{\partial}{\partial r} + \frac{\partial^2}{\partial \not{z}^2} \tag{19}$$

For radial symetry, this reduces to

$$\nabla 2 = \frac{\partial^2}{\partial r^2} + \frac{1}{r} \frac{\partial}{\partial r} + \frac{\partial^2}{\partial \not{z}^2} \tag{20}$$

With the boundary conditions of

a) no heat transfer at the ends, $\left.\frac{\partial T}{\partial Z}\right|_{\substack{Z = L \\ Z = o}} = 0$

b) no heat transfer at the outer radius, $\left.\frac{\partial T}{\partial r}\right|_{k = r_{\emptyset}} = 0$

c) heat loss, at inner radius, to liquid hydrogen

$$K \left.\frac{\partial T}{\partial r}\right|_{r = r_i} = - h \ (T - T_f) \qquad (21)$$

Neglecting the second order term, $\frac{\partial^2 T}{\partial Z^2}$,

The generalized equation can now be rewritten as

$$C_p \rho \frac{\partial T}{\partial t} = k \frac{\partial^2 T}{\partial r^2} + \frac{k}{r} \frac{\partial T}{\partial r} \qquad (22)$$

If the tube is thin walled, the conduction term $k \frac{\partial^2 T}{\partial r^2}$ will be small compared to losses at the boundary so that by virtue of boundary condition (C), the equation simplifies to

$$\frac{\partial T}{\partial t} = - \frac{h}{C_p \rho \delta} \quad (T - T_f) \tag{23}$$

where $\delta = \dfrac{D_o^2 - D_i^2}{4 D_i}$

By a rearrangement of the terms, the above equation can be written as

$$A \rho C_p \delta \frac{dT}{dt} = - h \ (T - T_f) A \tag{24}$$

where if A is considered as the inner surface of the tube. The left-hand side represents the rate of energy dissipation by the metal and the right side of the heat transferred to the fluid stream*.

---

*The same expression can be derived from a shell energy balance on the tube. For a hollow cylinder, adiabatically constrained on all surfaces except the inner one,

$$V = \pi \frac{D_o^2 - D_i^2}{4} L \qquad \text{and} \quad A = \pi D_i L$$

Defining $\delta = \dfrac{V}{A}$, then

$$\delta = \frac{D_o^2 - D_i^2}{4 D_i}$$

The question now arises as to the adequacy of data necessary to perform the integration of the equation. The specific heats are adequately covered in Reference 1 (WADC TR-60-56). The heat transfer coefficient h for liquid or two-phase hydrogen flow is presented in References 6 and 7. In the work of Hendricks, et.al., the correlation is presented on the basis of the Martinelli parameters with an error of 15%. Using a Leidenfrost correlation, the accuracy was comparable. Numerical integrations were then performed on the equation

$$t/\delta = -\int_{T_o}^{T} \Psi(T - T_f)\, d\,T \qquad (25)$$

where

$$\Psi(T - T_o) = \frac{\rho C_p}{h\,(T - T_f)} \qquad (26)$$

if T_f, the fluid temperature is the equilibrium temperature of boiling hydrogen, T_L, then the implied initial condition becomes

$$T_f = T_o \qquad t < 0$$

$$T_f = T_L \qquad t > 0$$

and the integral equation takes the form

$$t/\delta = -\int_{T_o}^{T} \Psi(T - T_L)\, d\,T \qquad (27)$$

On Figures 23, 24, and 25 the integrations of Equation 27 for copper, aluminum and beryllium test sections are shown. Comparisons are also given for the case where an arithmetic mean specific heat between 40°R and 540°R is used, as well as the experical expression for $h = 3.56\,(T - T_e)^{1/4} \times 10^{-4}$ BTU/in^2 - sec.

1.2 TIME CONSTANT DEFINITION

In order to provide a criteria for the comparison of experimental data, with the computer-determined cool-down results, it is assumed that $h/\rho C_p$ is a constant. Hence Equation 24 can be integrated directly to give

$$T - T_L = (T_o - T_L) = e^{-\frac{h\,t}{\rho C_p \delta}} \qquad (28)$$

This type of exponential process is usually discussed in terms of one of two types of characteristic times. Nuclear processes refer to "half life", and electrical process refer to a "time constant". Each in turn can be defined as:

1. Half life: value of t such that

$$T - T_L / T_o - T_L = 1/2 = e^{-\frac{h}{\rho C_p \delta}\, t} \qquad (29)$$

so that for an exponential cooling curve:

$$t = .694\ C_p \rho\delta/h$$

and

2. Time constant: value of t such that

$$T - T_L/T_o - T_L = e^{-1} = e^{-\frac{h}{\rho C_p \delta} t} \qquad (30)$$

so that for an exponential cooling curve, the time constant or

$$t' = \rho C_p \delta/h \qquad (31)$$

In this report the time constant t' is based on the second definition, that is the time required for the temperature difference to attain e^{-1} (36.8%) of the maximum temperature difference. It should be noted that only for an exponential curve (which implies C_p, ρ, and h are constant) is the value given by Equation 31 valid.

1.3 CORRECTIONS FOR FLOW DELAYS

The general cool-down curves presented in Figure 5 have implied, as an initial condition, a step function in the temperature of the coolant fluid. At time $t < 0$ the interior of the tube is at T_o and at $t > 0$ the interior is at T_t taken as the boiling point of the coolant. In the experiments performed to date, a significant length of time elapsed before the coolant temperature reached the boiling point. Hence Equation 24 must now be considered with T_f a function of t. For an approximation an exponential function of T_f was assumed:

$$T_f = (T_o - T_L)e^{-Bt} + T_L \tag{32}$$

where T_L is the boiling point of liquid hydrogen. Substituting this value in Equation 24 gives

$$C\rho\delta\frac{dT}{dt} = h\left(T - \left\{(T_o - T_L)e^{-Bt} + T_L\right\}\right) \tag{33}$$

By rearranging, the following linear equation is obtained:

$$\frac{dT}{dt} + \frac{h}{C\rho\delta}(T - T_L) = \frac{h}{C\rho\delta}(T_o - T_L)e^{-Bt} \tag{34}$$

The equation can be solved by the integrating factor to give

$$T - T_L = e^{-\frac{h}{C\rho\delta} t} \left(\frac{h}{C\rho\delta} (T_o - T_L) \int e^{\left(\frac{h}{C\rho\delta} - B\right) t} dt + G \right) \quad (35)$$

For the initial condition that $T = T_o$ at $t = 0$ the equation becomes

$$\frac{T - T_L}{T_o - T_L} = \frac{e^{-\frac{h\,t}{\rho C\delta}} - e^{-B\,t}}{1 - \frac{h}{\rho C\,\delta\,B}} \quad (36)$$

The time constant associated with the fluid temperature is

$$t_f^1 = \frac{1}{B} \quad (37)$$

Similarly, the time constant of the tube has been defined by Equation 31. With the lag introduced by the progressive rather than instantaneous drop to the boiling point of the coolant the effective time constant t_e can be defined and experimentally obtained as the time required for

$$\frac{T - T_L}{T_o - T_L} \quad \text{to reach} \quad \frac{1}{e}$$

Combining Equations 31, 36, and 37:

$$\frac{1}{e} = \frac{e^{-\frac{t_e}{t'}} - \frac{t_f'}{t'} e^{-\frac{t_e}{t_f'}}}{1 - \frac{t_f'}{t_e}} \qquad (38)$$

Since t_e and t_f' can be measured from experimental data, t' can be deduced as the corrected time constant equivalent to the instaneous drop of the entering coolant to the boiling point.

If t_f' and t_e are known, t' can be calculated from Equation 38.

1.4 VOID FRACTIONS

Let it be assumed that in mist flow and slug flow, the liquid flows as individual plugs, the plugs being very thin in mist flow. Further, assume that vapor film thicknesses around the liquid plugs are negligible. This model implies that at any instant, vapor and liquid velocities are equal. Then for any differential time increment d t, the differential sum of liquid residence times divided by the differential time gives the average volume fraction liquid in this time increment:

$$v_L = 1 - \epsilon = \frac{d\,t_L}{d\,t} \qquad (39)$$

Therefore, the void fraction

$$\epsilon = 1 - \frac{d\,t_L}{d\,t} \qquad (40)$$

By definition, the time-averaged local instantaneous mass fraction vapor can be calculated from the equation

$$\bar{y}_t = \frac{\bar{\rho}_v \epsilon}{\bar{\rho}_v \epsilon + (1 - \epsilon)\rho_L} \tag{41}$$

The vapor density, $\bar{\rho}_v$ can be determined from the average vapor temperature.

1.4.1 EXIT VAPOR FRACTIONS

In view of the relatively high conductivity of copper and the thin wall of the tubing, the average instantaneous heat flux from the wall to the fluid can be defined as

$$\overline{Q} = \frac{\pi}{4}\rho\left(D_o^2 - D_i^2\right) L \overline{C_p \frac{dT_w}{dt}} \tag{42}$$

where L is the length of the test section, D_o and D_i are outside and inside tube diameters. The slope $\frac{dT_w}{dt}$ for the inlet and exit of the test section can be determined by either graphical or numerical differentiation of the local wall temperature histories. A linear enthalpy change with time can be assumed, whence

$$\overline{C_p \frac{dT_w}{dt}} = \frac{\left(C_p \frac{dT_w}{dt}\right)_1 + \left(C_p \frac{dT_w}{dt}\right)_2}{2} \tag{43}$$

The subscripts 1 and 2 refer to the inlet and outlet of the test section, respectively. For an approximation, it is assumed that all the heat transferred to the two-phase fluid is used to vaporize the liquid. The vapor fraction at the exit can then be calculated from the average heat flux by the following relationship:

$$y_2 = y_1 + \frac{\overline{Q}}{\lambda W} \qquad (44)$$

where λ is the latent heat of vaporization and W is the instantaneous mass flowrate.

1.4.2 ALTERNATE METHOD FOR ESTIMATING AVERAGE VAPOR FRACTIONS

It was noted from the data that for some runs, a time lag clearly existed between the inlet and exit temperature traces. The distance between the two locations divided by the time lag, τ, gives the instantaneous average two-phase fluid velocity in the test section, V_{TP}. By definition, the instantaneous average two-phase fluid density over the test section is given by

$$\rho_{TP} = \frac{W_{TP}}{V_{TP} S} \qquad (45)$$

where W_{TP} is the mass flowrate, and S is the inside tube cross-sectional area.

It follows that the average mass fraction vapor over the tube, $\bar{y}$, can be computed from the equation

$$\bar{y} = \frac{\bar{\rho}_v \epsilon}{\bar{\rho}_{TP}} \qquad (46)$$

Based on a unit volume of two-phase fluid, the average two-phase fluid density is related to the vapor and liquid densities by the equation

$$\bar{\rho}_{TP} = \bar{\rho}_v \quad \epsilon + \quad \rho_L \quad (1 - \epsilon)$$

or

$$\epsilon = \frac{\rho_L - \bar{\rho}_{TP}}{\rho_L - \bar{\rho}_v} \qquad (47)$$

Substituting into 46 , the Equation becomes

$$\bar{y} = \frac{\bar{\rho}_v \left| \rho_L - \bar{\rho}_{TP} \right|}{\bar{\rho}_{TP} \left| \rho_L - \bar{\rho}_v \right|} \qquad (48)$$

If the average instantaneous fluid velocity is known, then the average fluid density can be determined from Equation 47, and the vapor fraction can be computed from Equation 48.

FIGURE 1
HYDROGEN TEST FACILITY

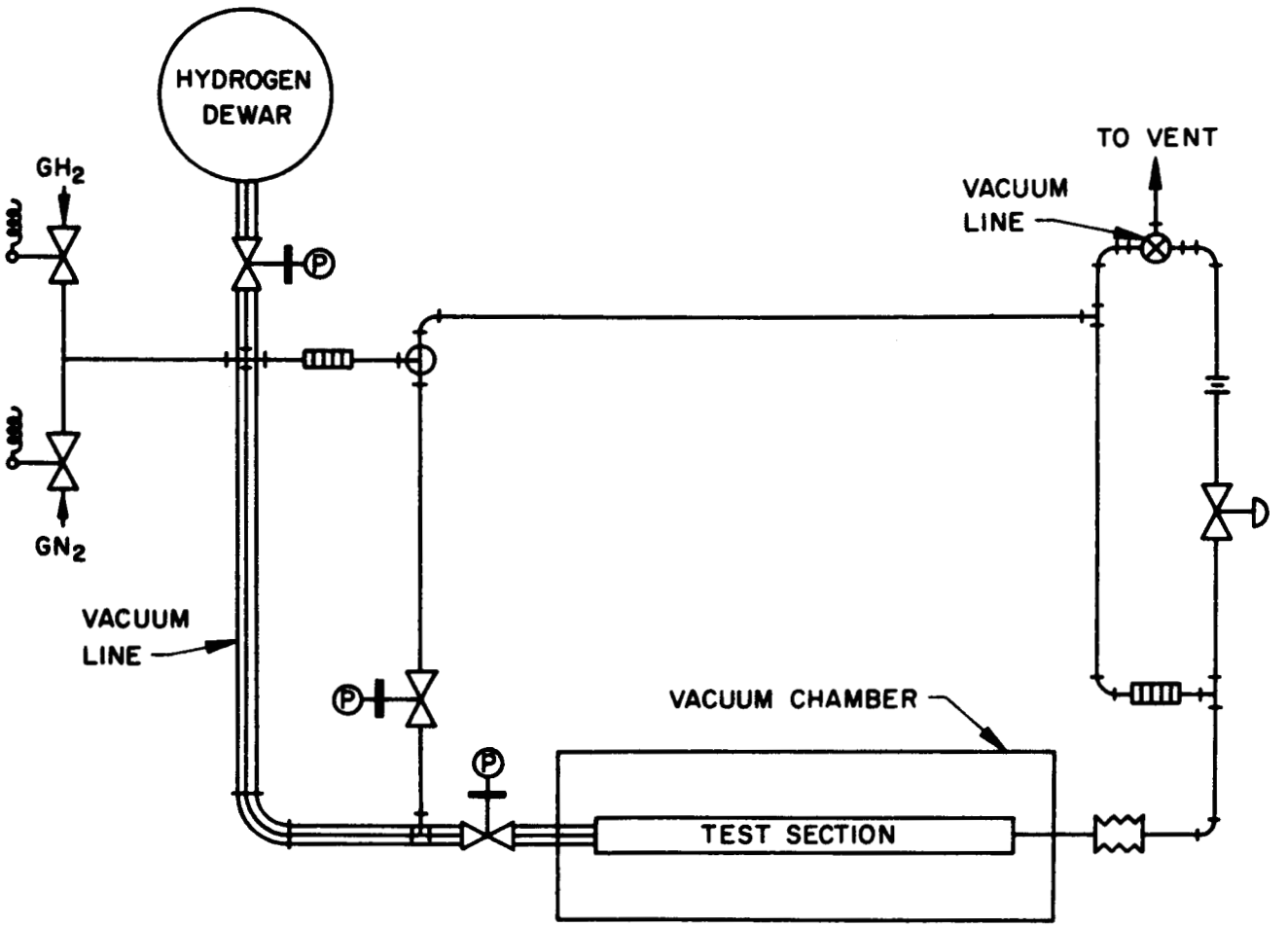

FIGURE 2 - SCHEMATIC DIAGRAM OF THE HYDROGEN TEST LOOP

560760

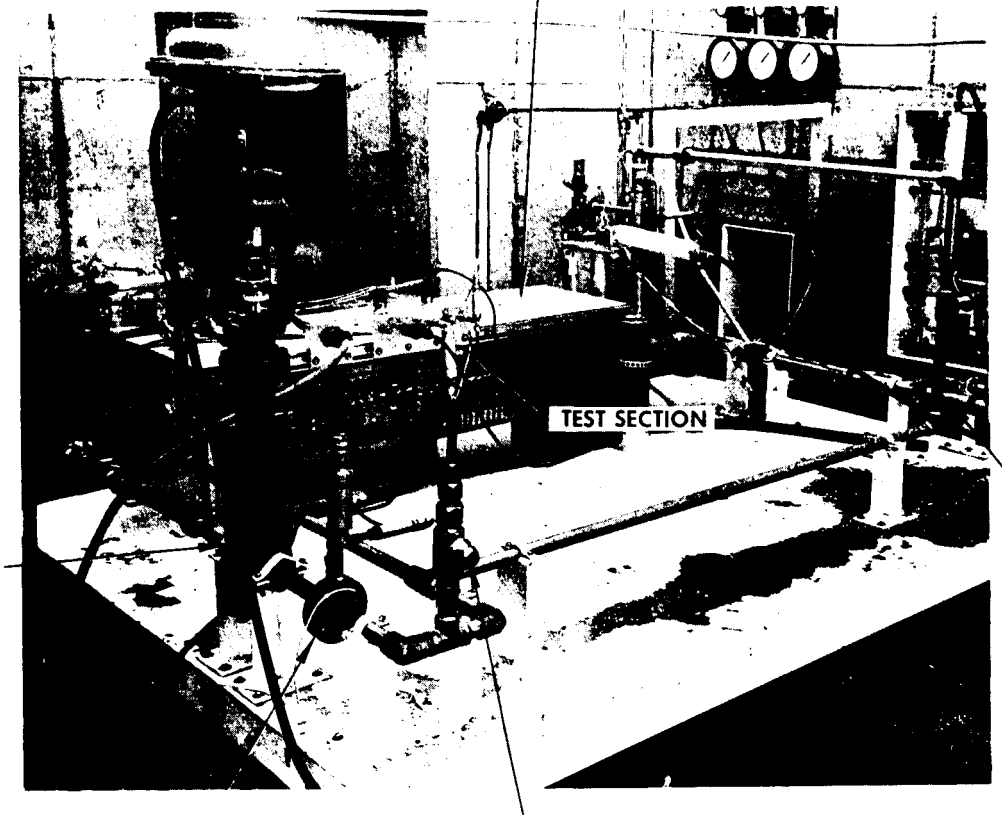

FIGURE 3

HYDROGEN TEST LOOP

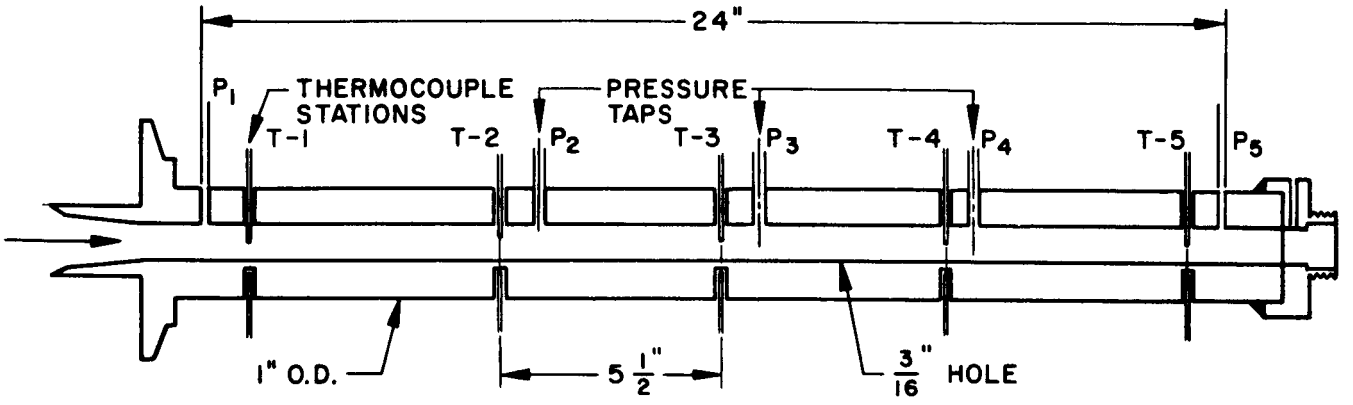

(a) ALUMINUM

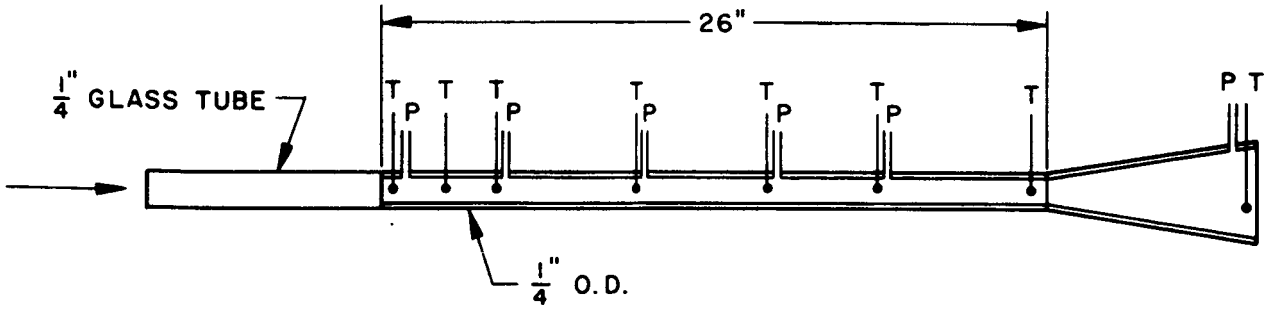

(b) COPPER

FIGURE 4 - SCHEMATIC DIAGRAM OF TEST SECTIONS

560761

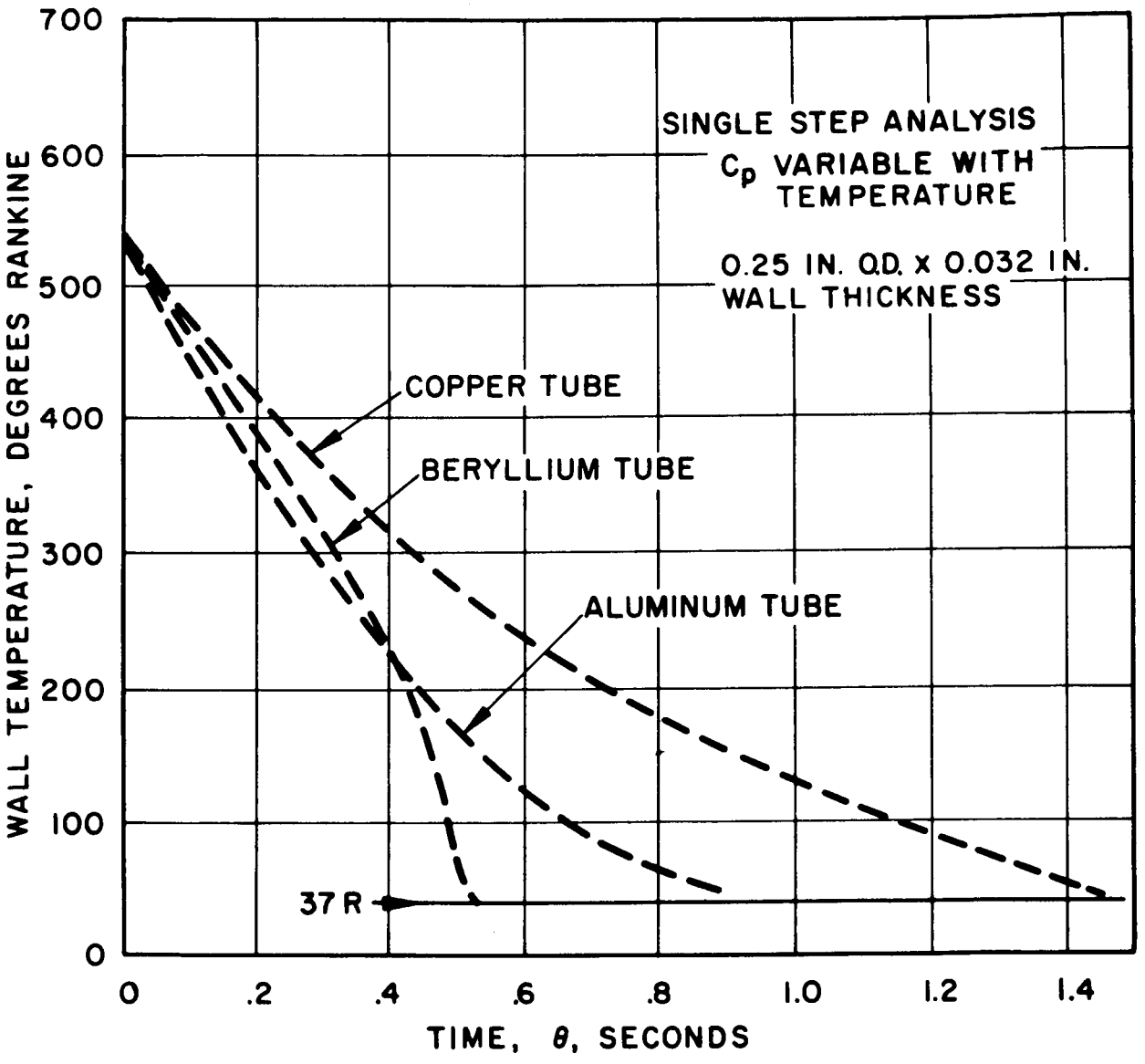

FIGURE 5 – RESULTS OF SINGLE STEP ANALYSIS OF TRANSIENT TEMPERATURE HISTORY WITH HYDROGEN FLOW IN A THIN WALLED TUBE

560762

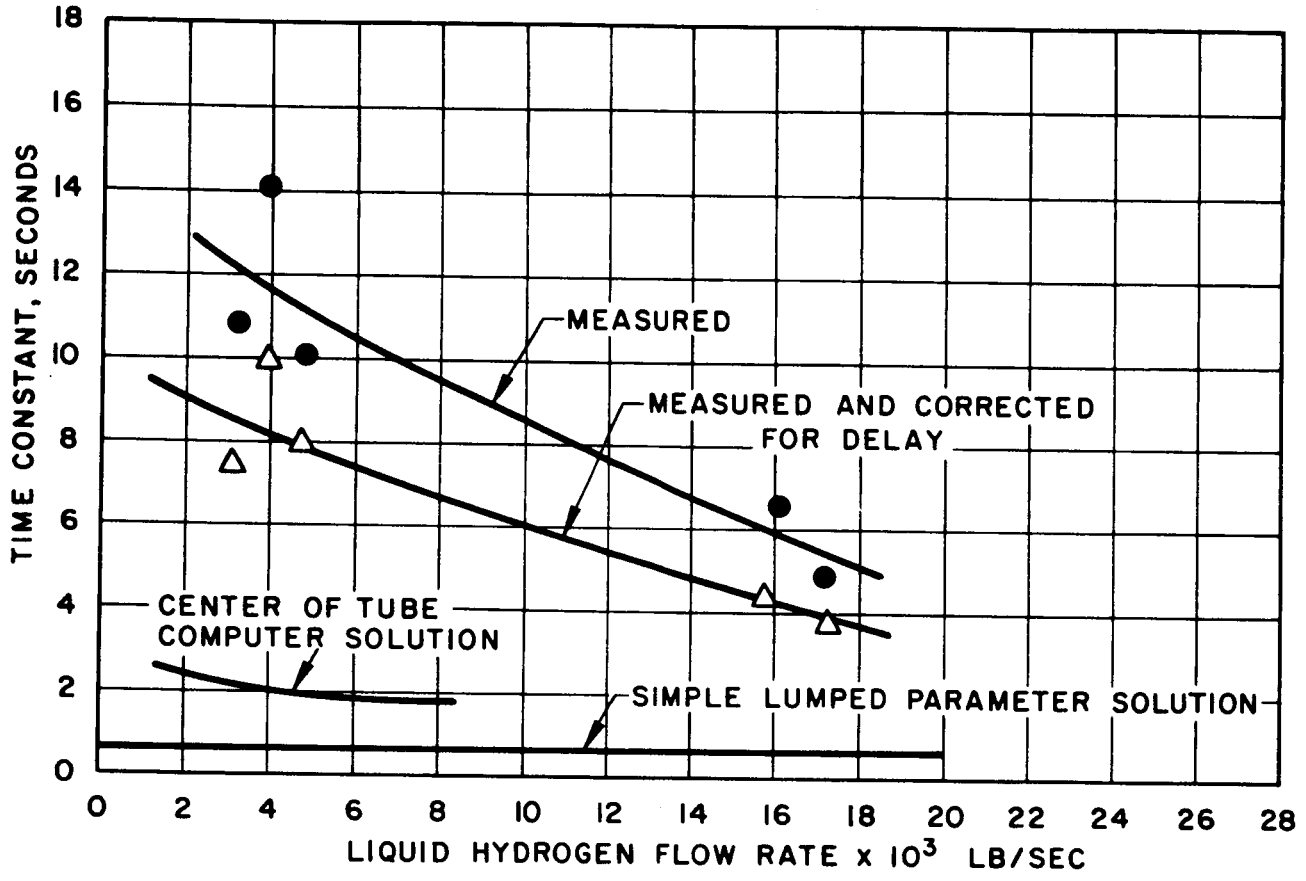

FIGURE 6 - EFFECT OF FLOW RATE ON TIME CONSTANT FOR 0.1875 IN I.D. COPPER TUBE

560763

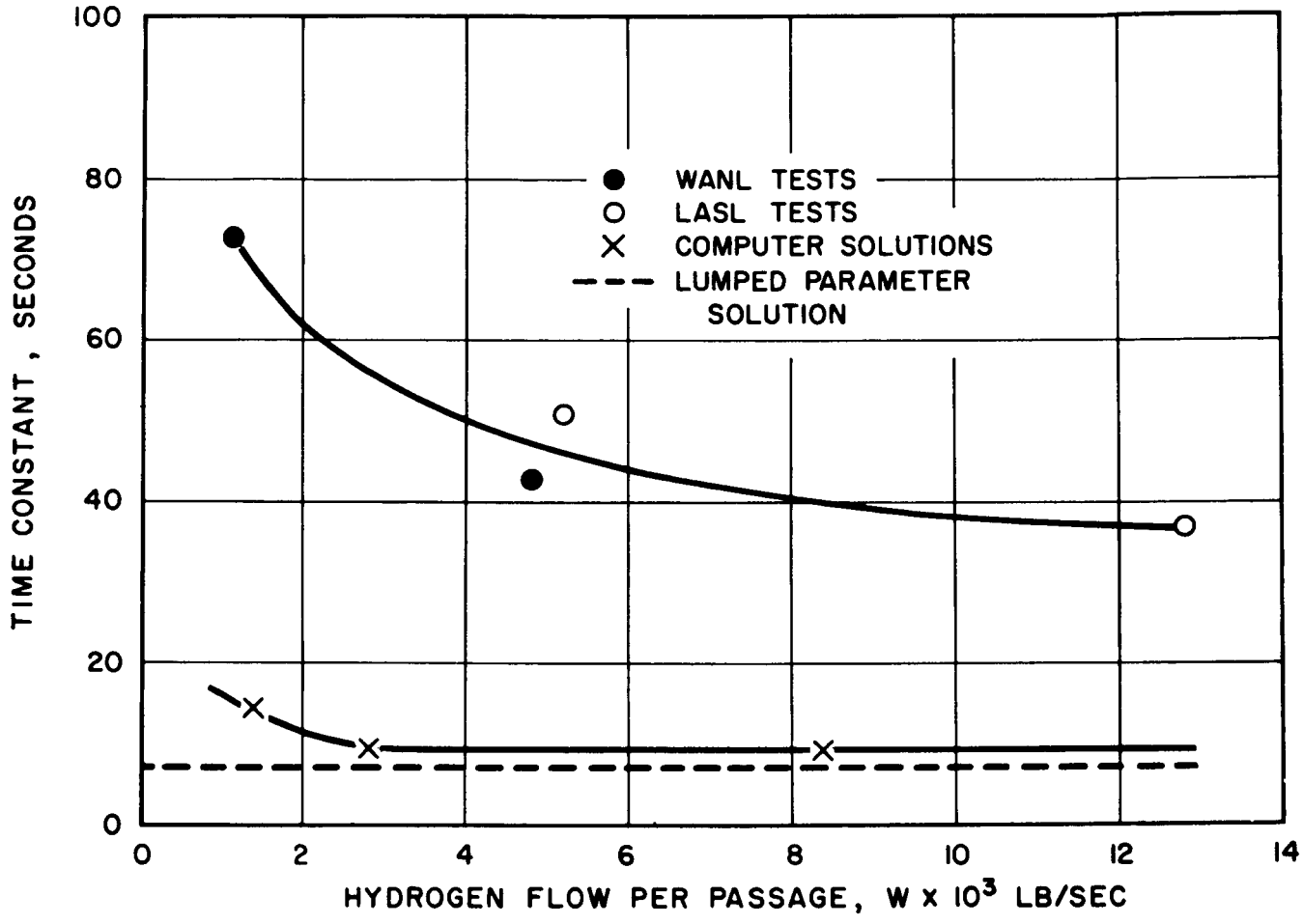

FIGURE 7- EFFECT OF FLOWRATE ON TIME CONSTANTS FOR 0.1875 IN. I.D. ALUMINUM TUBE

560764

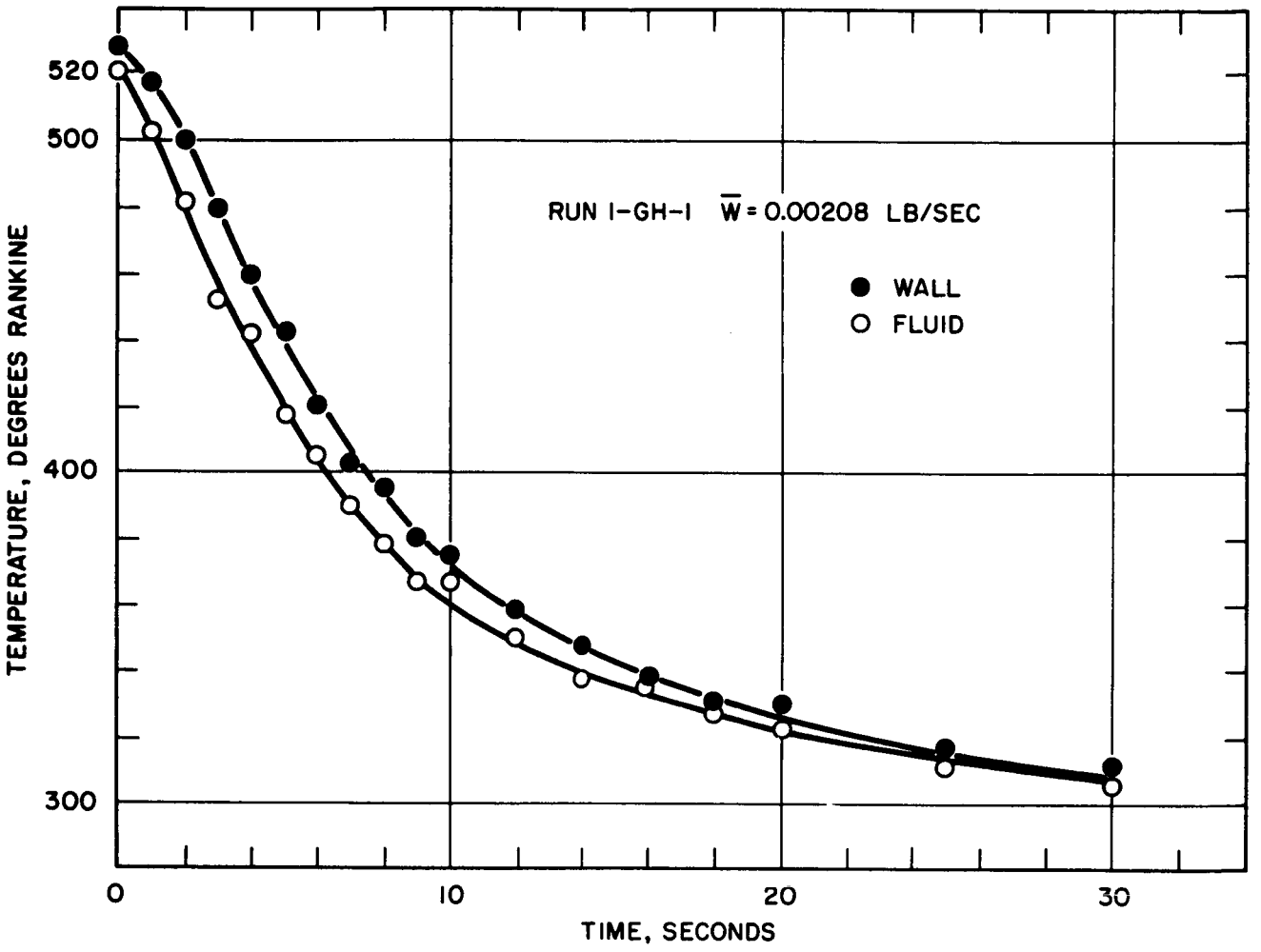

FIGURE 8 – TEST SECTION WALL AND FLUID TEMPERATURE HISTORIES

560765

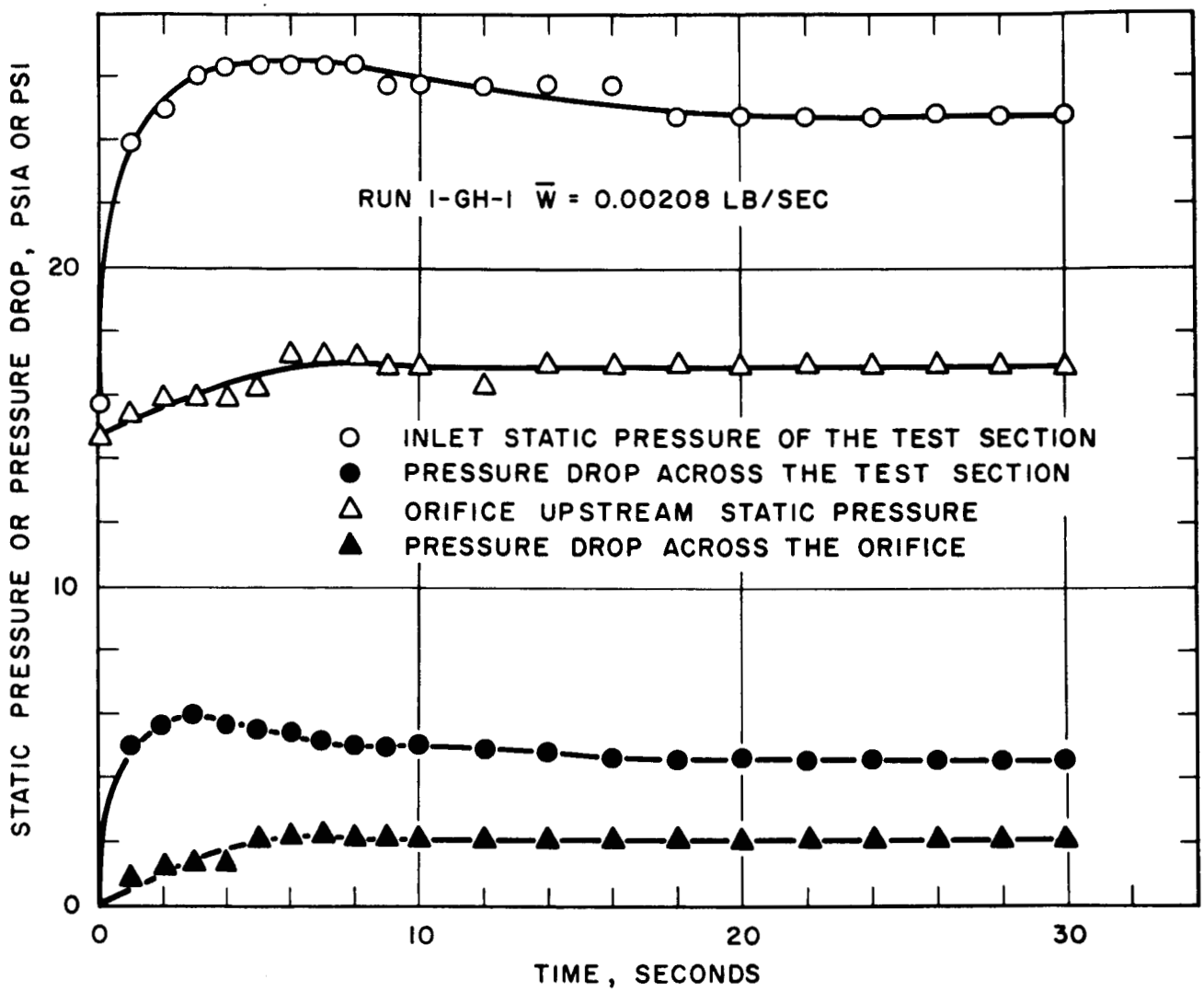

FIGURE 9 - PRESSURE AND PRESSURE DROP HISTORIES 560766

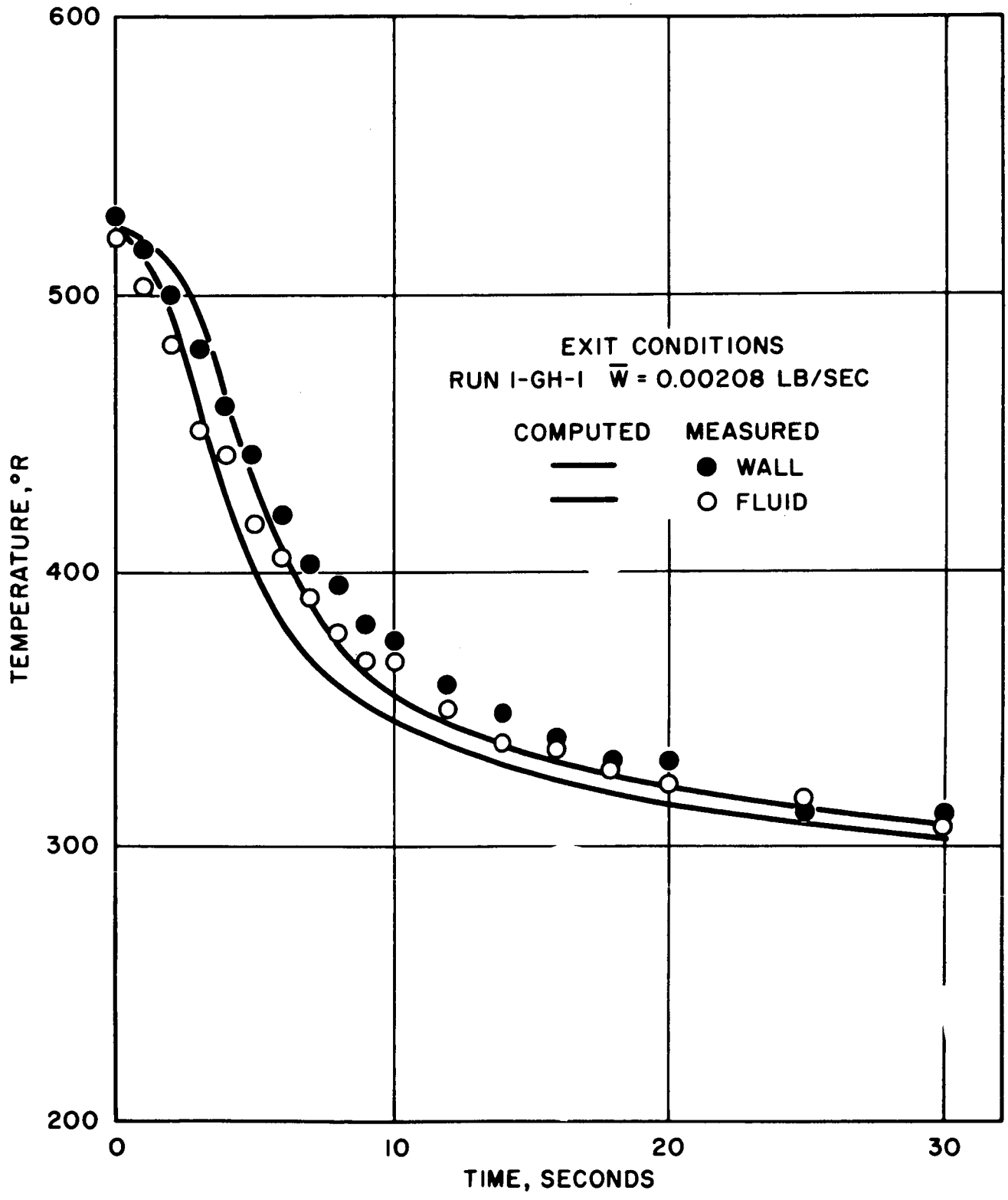

FIGURE 10-COMPARISON OF COMPUTER PREDICTED AND EXPERIMENTAL FLUID TEMPERATURES AT EXIT OF THE TEST SECTION

560767

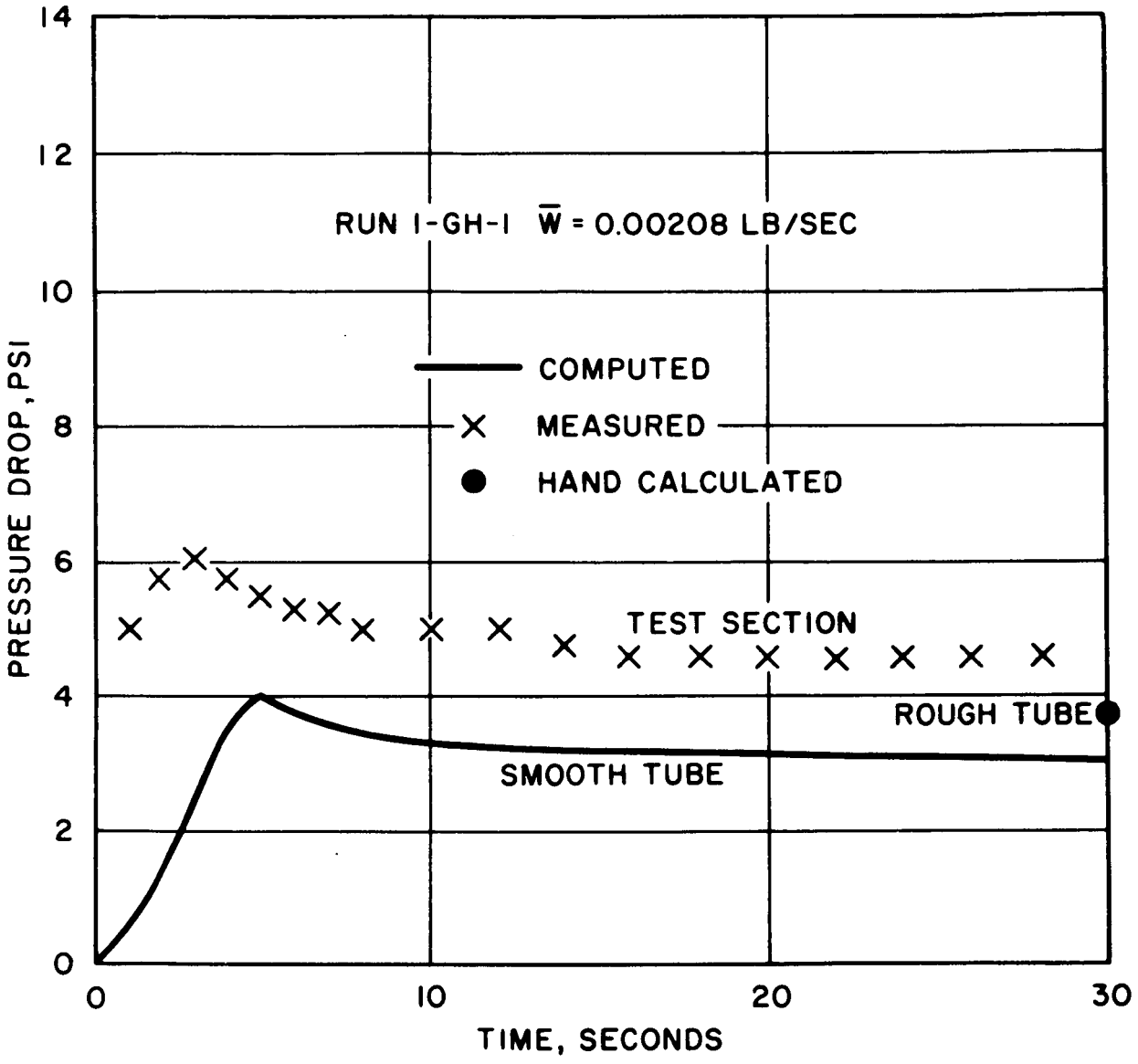

FIGURE 11 - COMPARISON OF CALCULATED AND MEASURED PRESSURE DROPS ACROSS THE TEST SECTION

560768

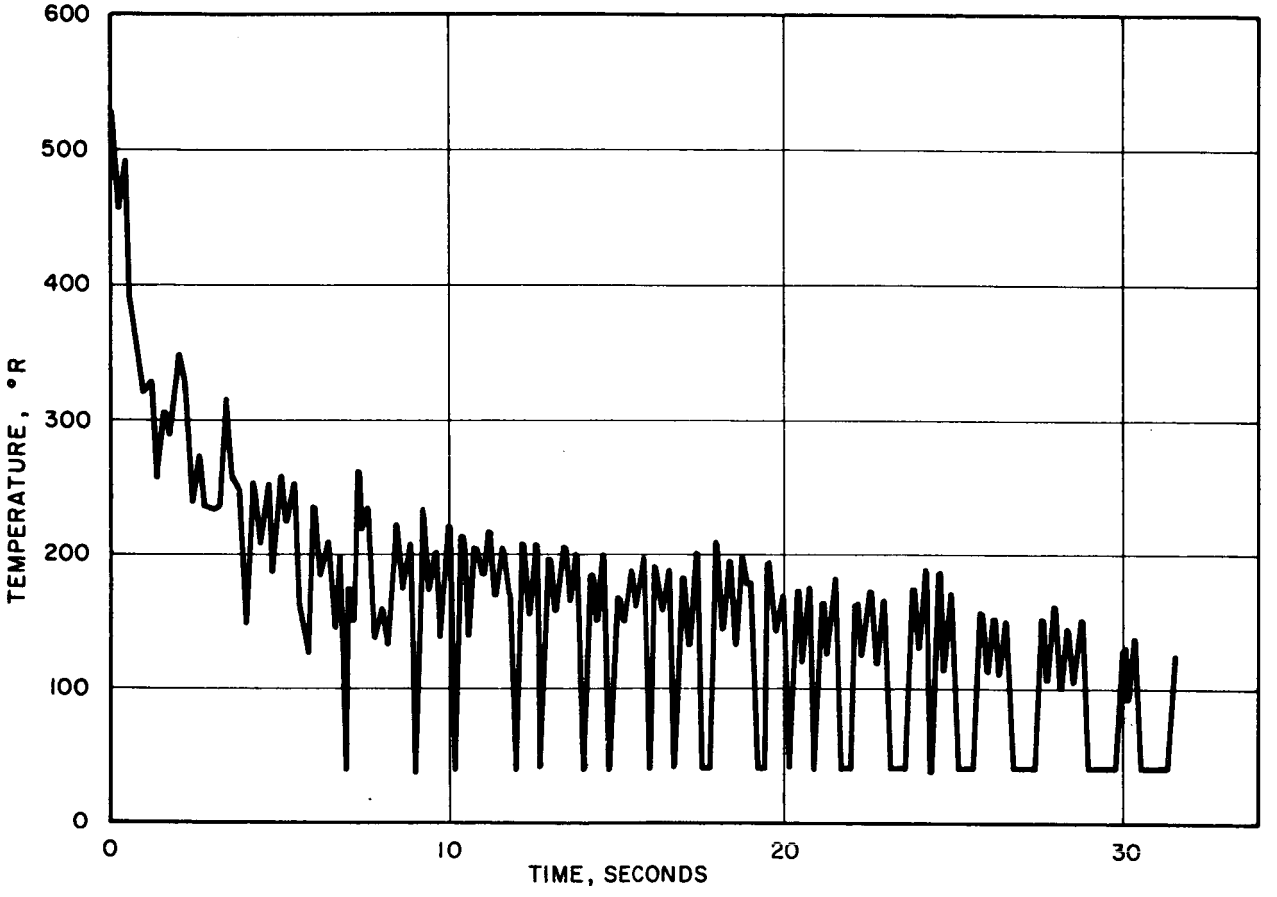

FIGURE 12– TYPICAL INLET STREAM TEMPERATURE HISTORY

560630

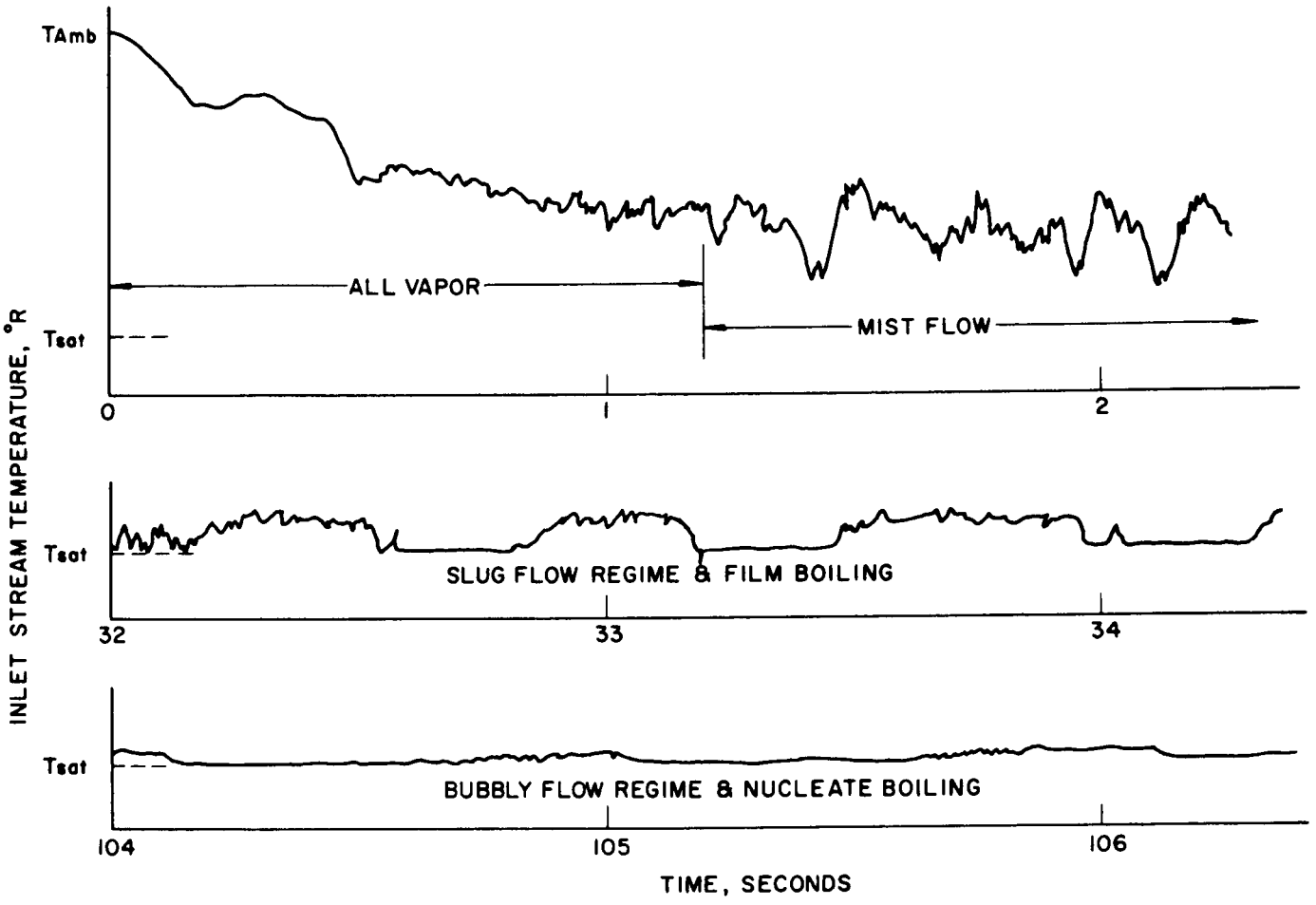

FIGURE 13-VISICORDER TEMPERATURE TRACES SHOWING VARIOUS FLOW REGIMES DURING COOL-DOWN 560924

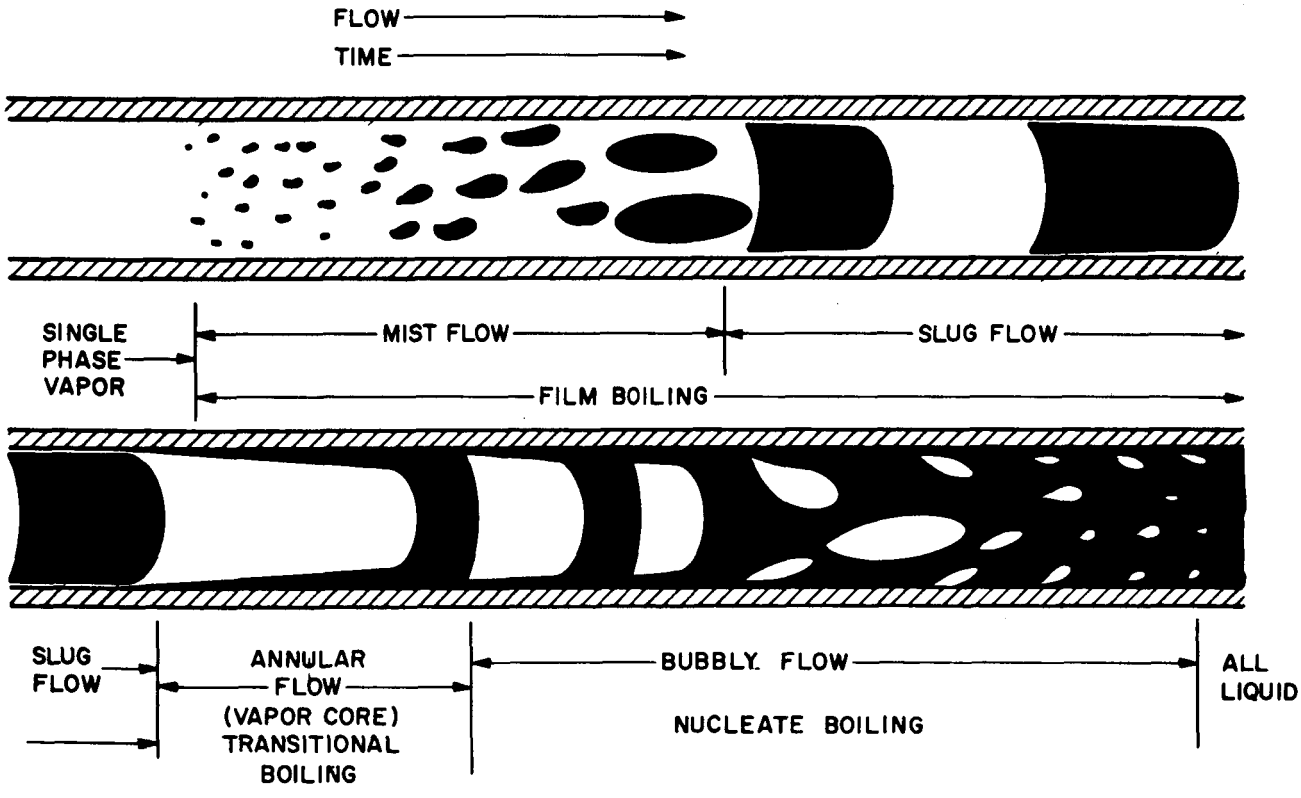

FIGURE 14- SCHEMATIC DIAGRAM ON THE VARIOUS MODES OF TWO PHASE FLOW AND HEAT TRANSFER REGIMES AT A FIXED POSITION

560631

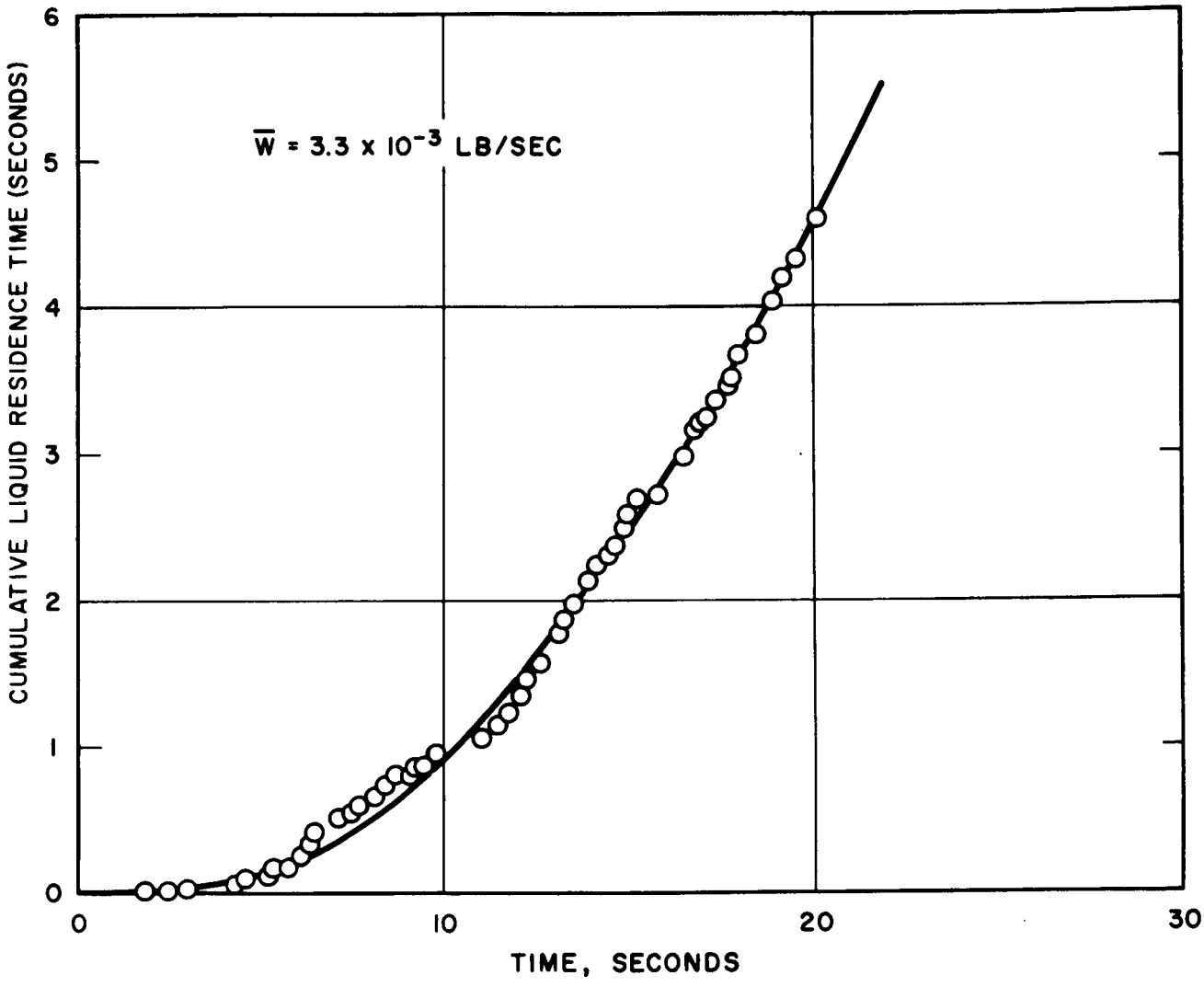

FIGURE 15 - TYPICAL LIQUID RESIDENCE TIME HISTORY 560772

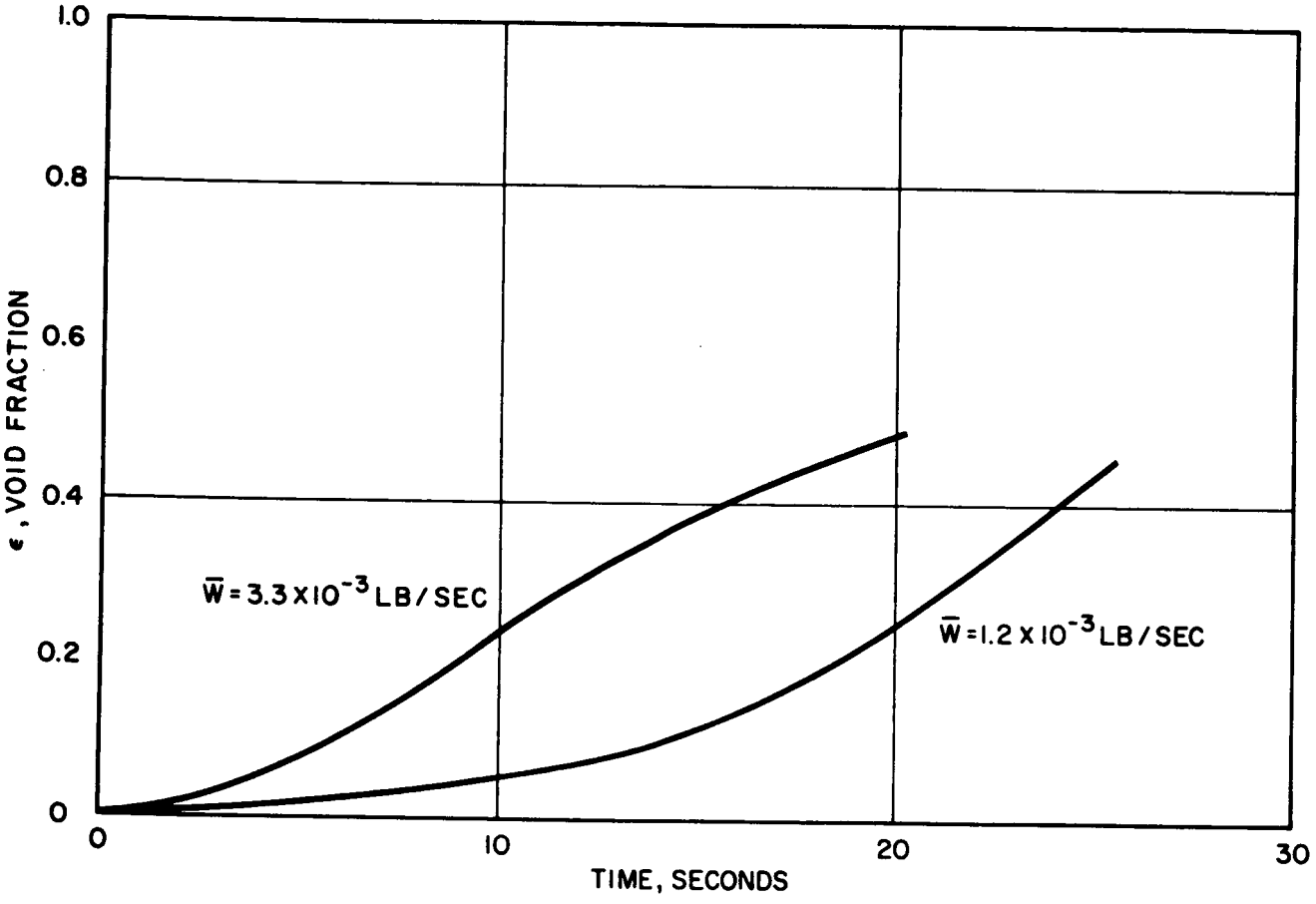

FIGURE 16-PROBABILITY OF MEASURING LIQUID TEMPERATURES

560773

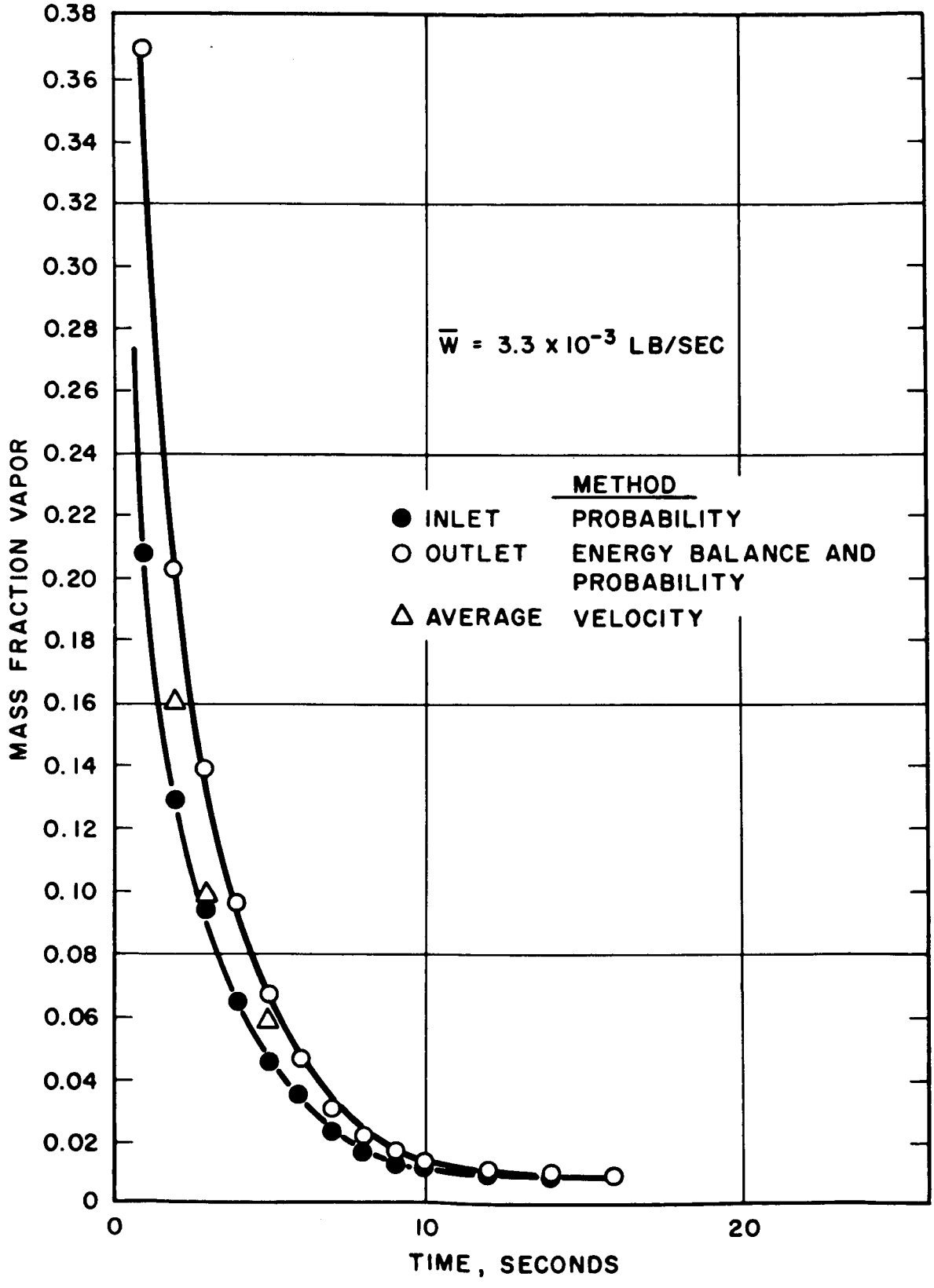

FIGURE 17. COMPARISON OF CALCULATED VAPOR FRACTIONS

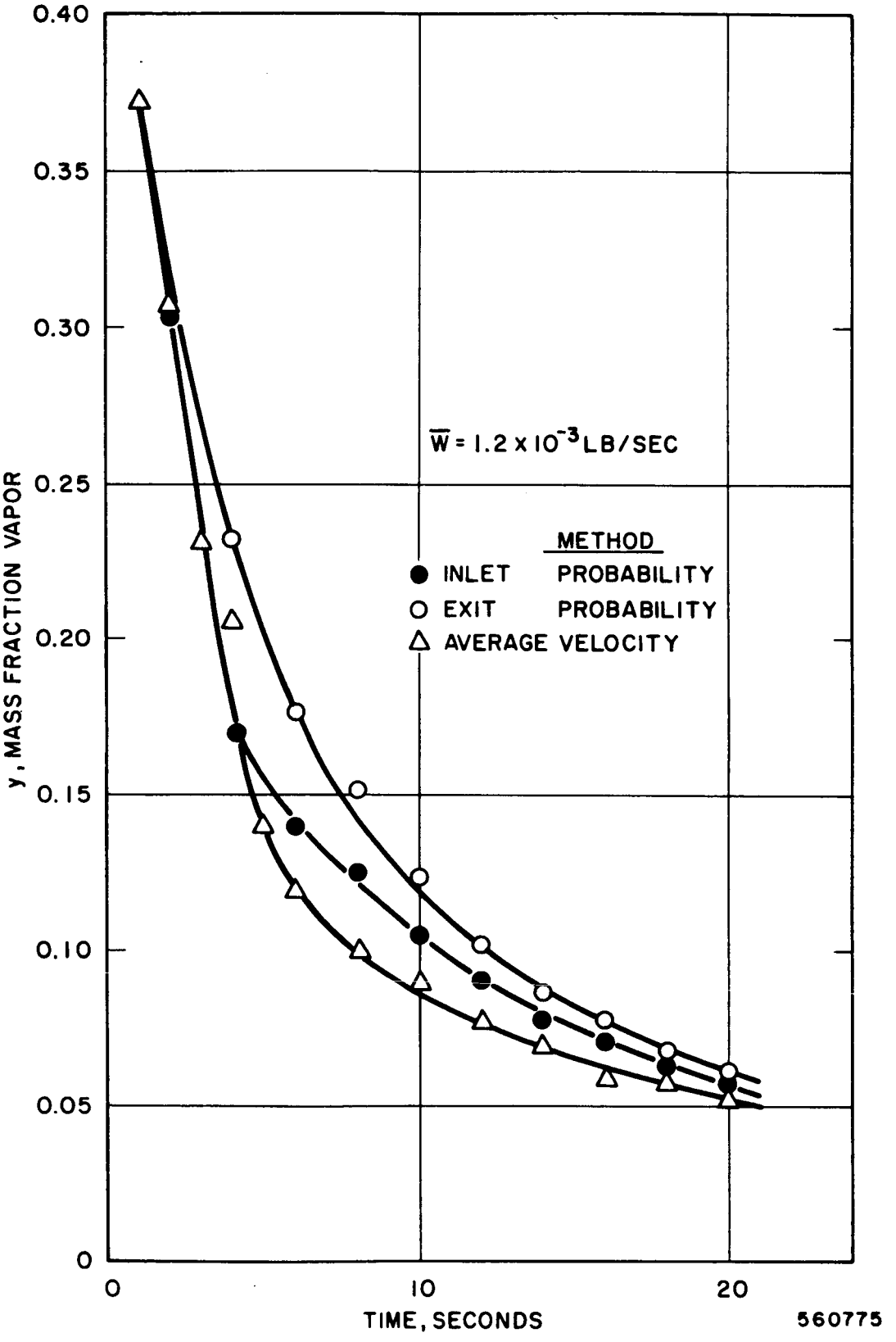

FIGURE 18. COMPARISON OF CALCULATED VAPOR FRACTIONS

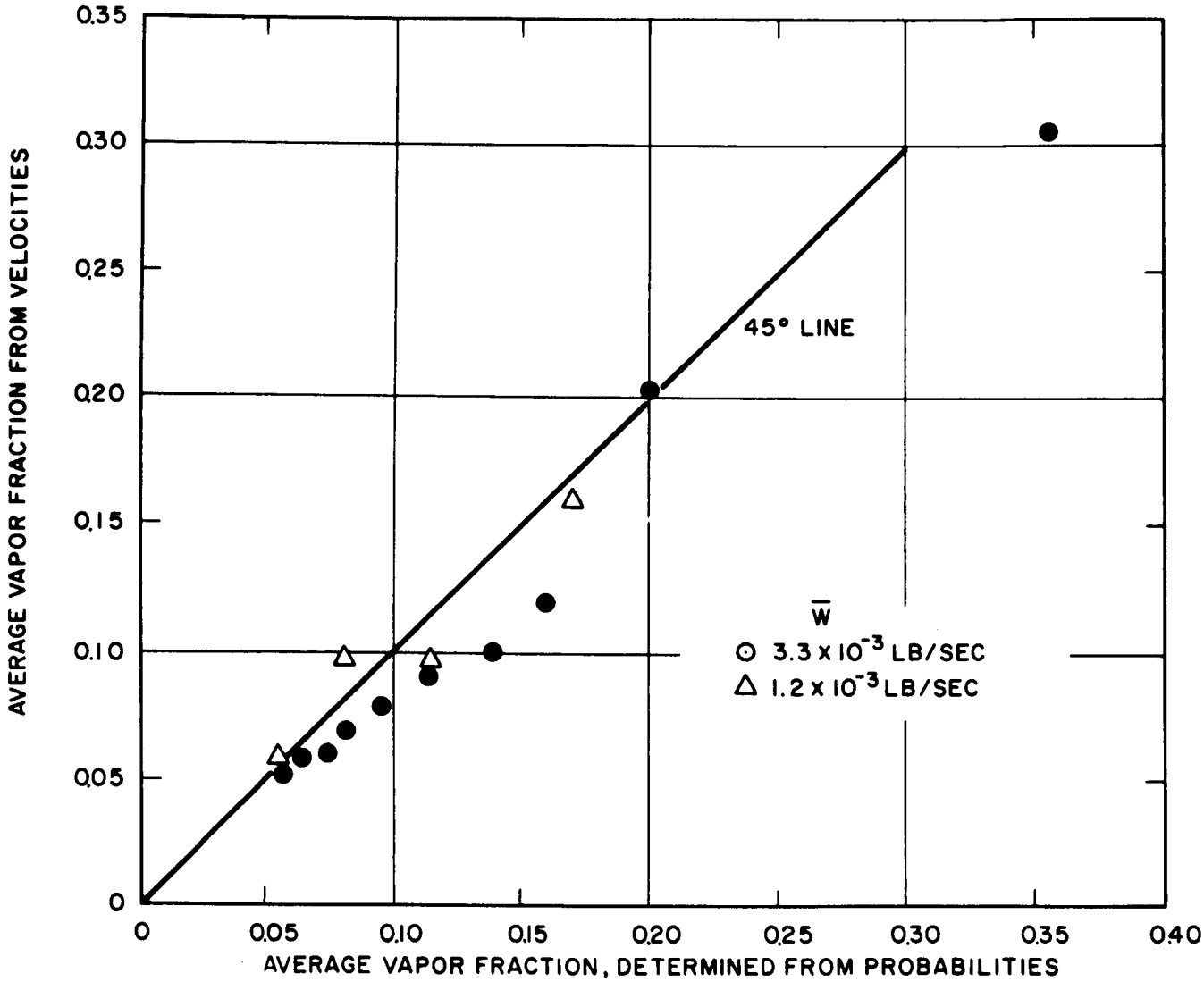

FIGURE 19 - COMPARISON OF AVERAGE VAPOR FRACTIONS DETERMINED BY TWO METHODS

560776

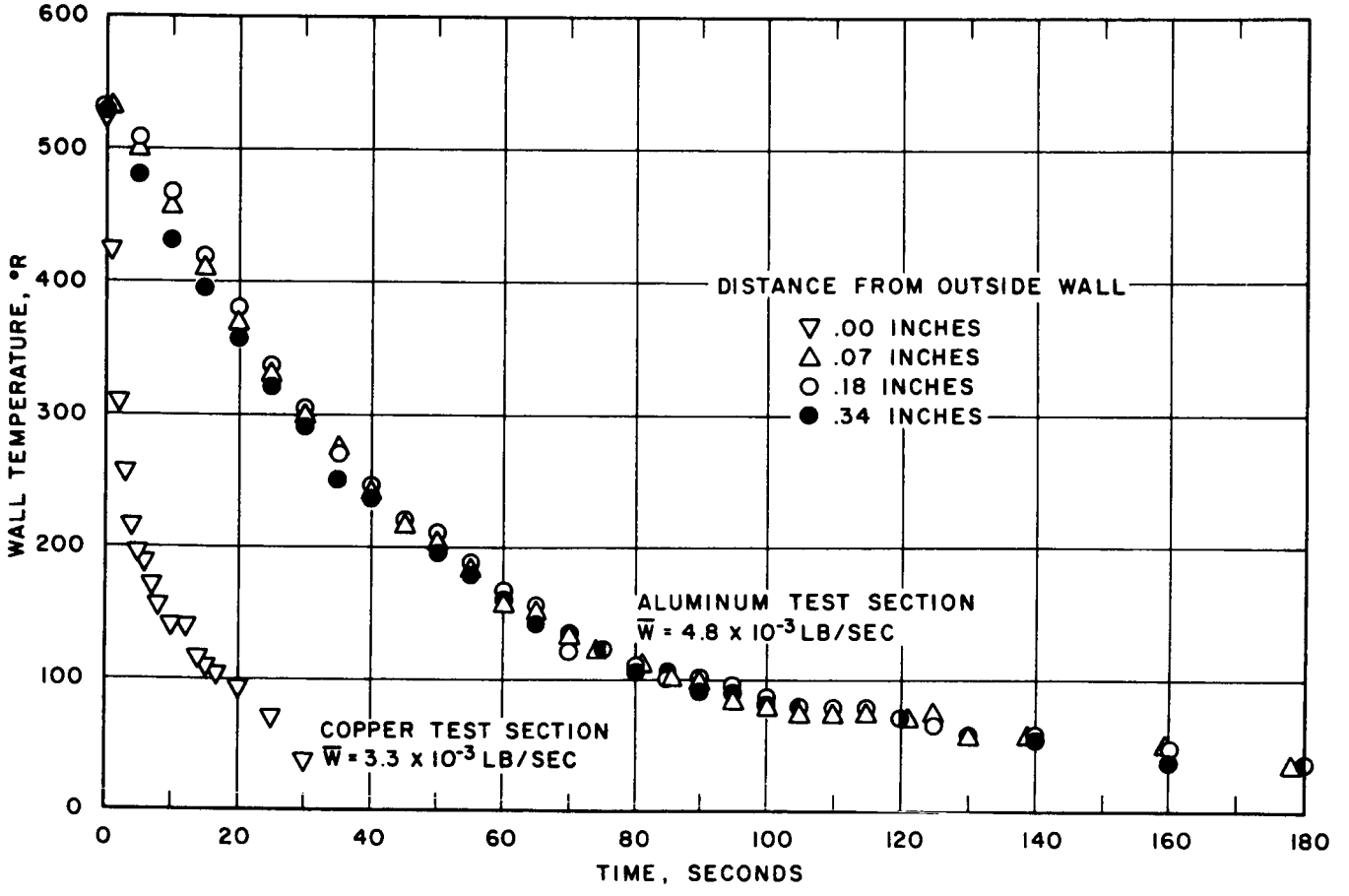

FIGURE 20. TYPICAL WALL TEMPERATURE HISTORIES DURING COOL DOWN OF COPPER AND ALUMINUM TEST SECTIONS

560777

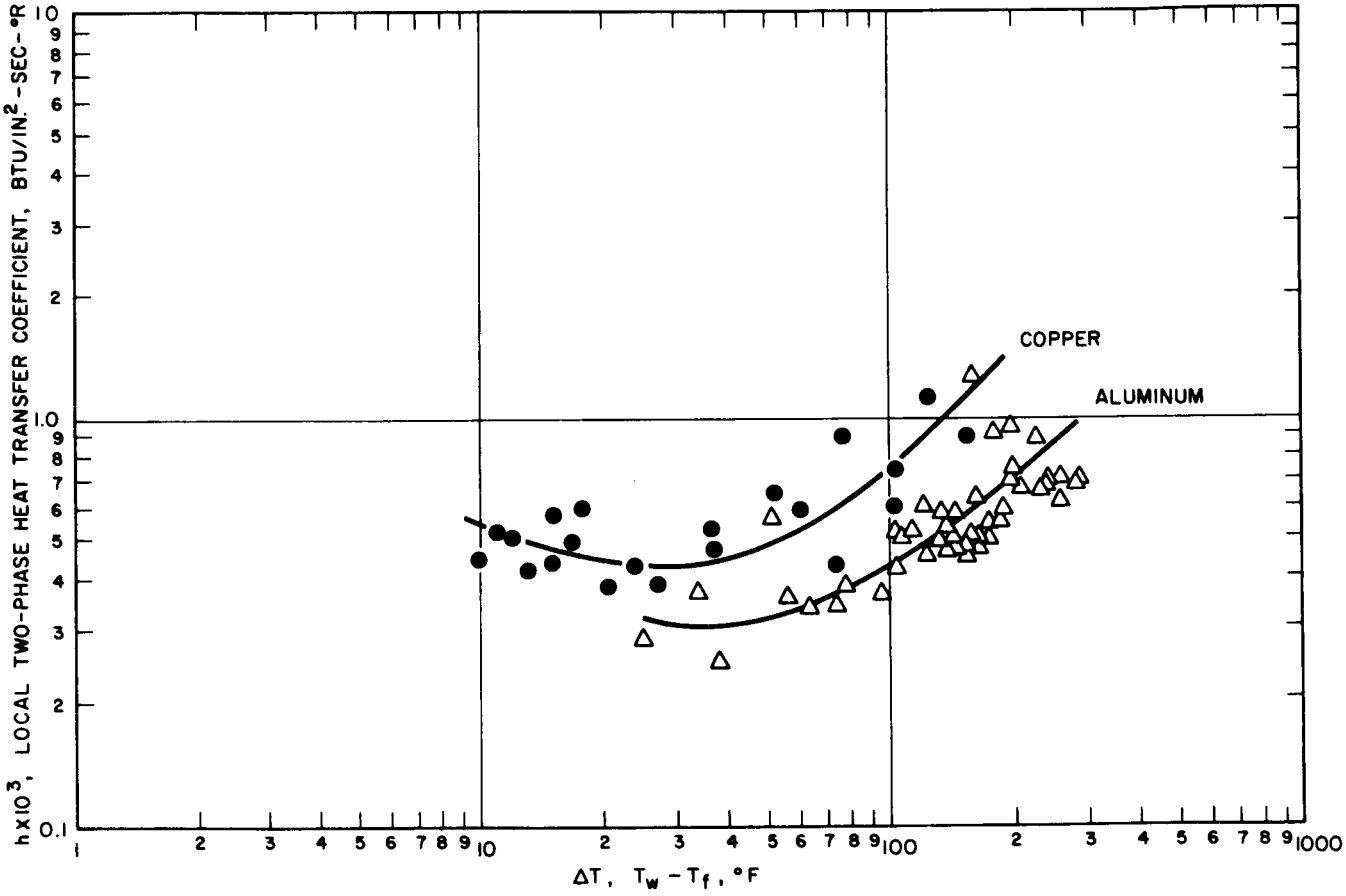

FIGURE 21. COMPARISON OF FILM BOILING HEAT TRANSFER COEFFICIENTS DETERMINED FROM COPPER AND ALUMINUM TEST SECTIONS

560778

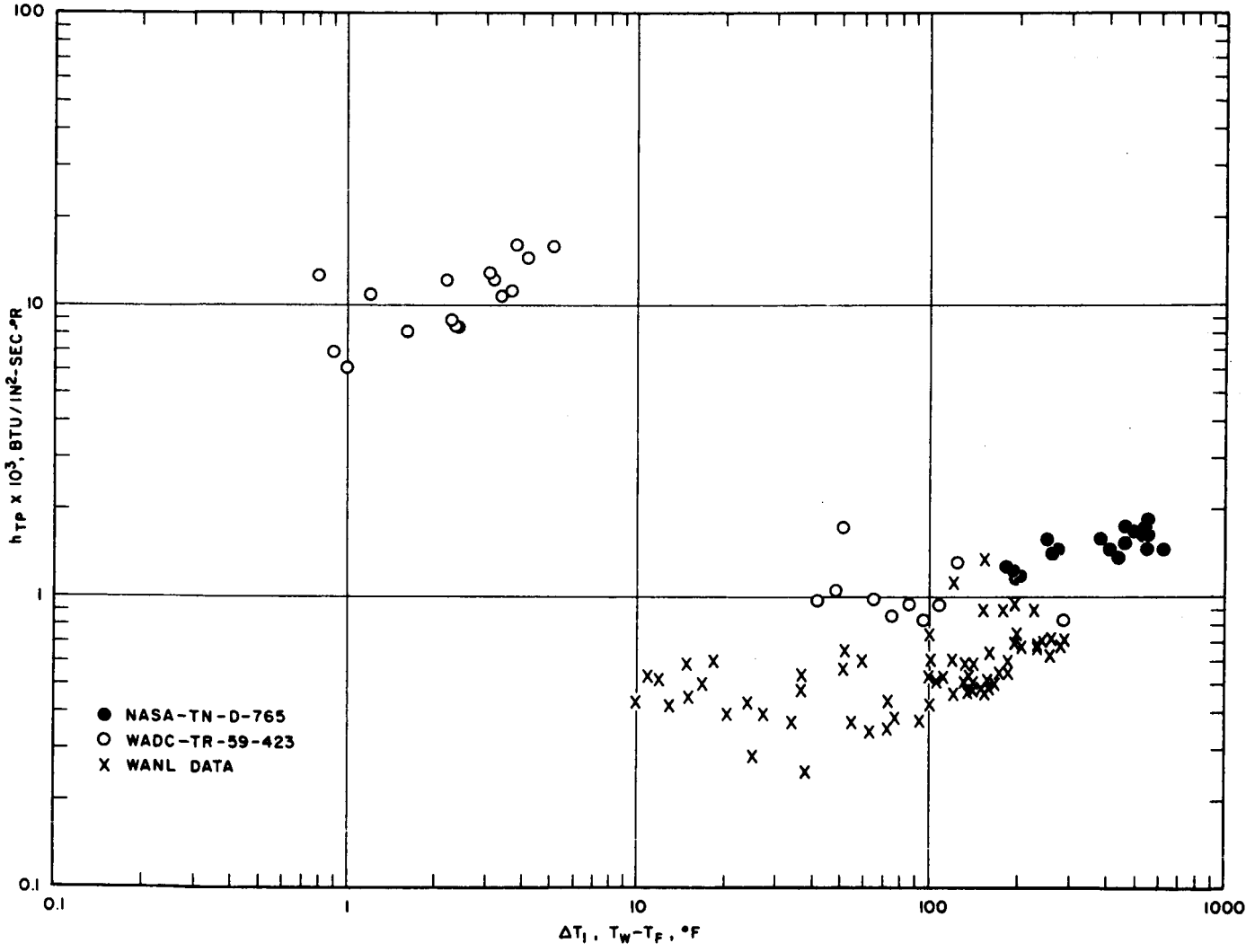

FIGURE 22 - COMPARISON OF TWO-PHASE HEAT TRANSFER COEFFICIENTS FROM VARIOUS SOURCES FOR HYDROGEN

CURVE NO. 560779

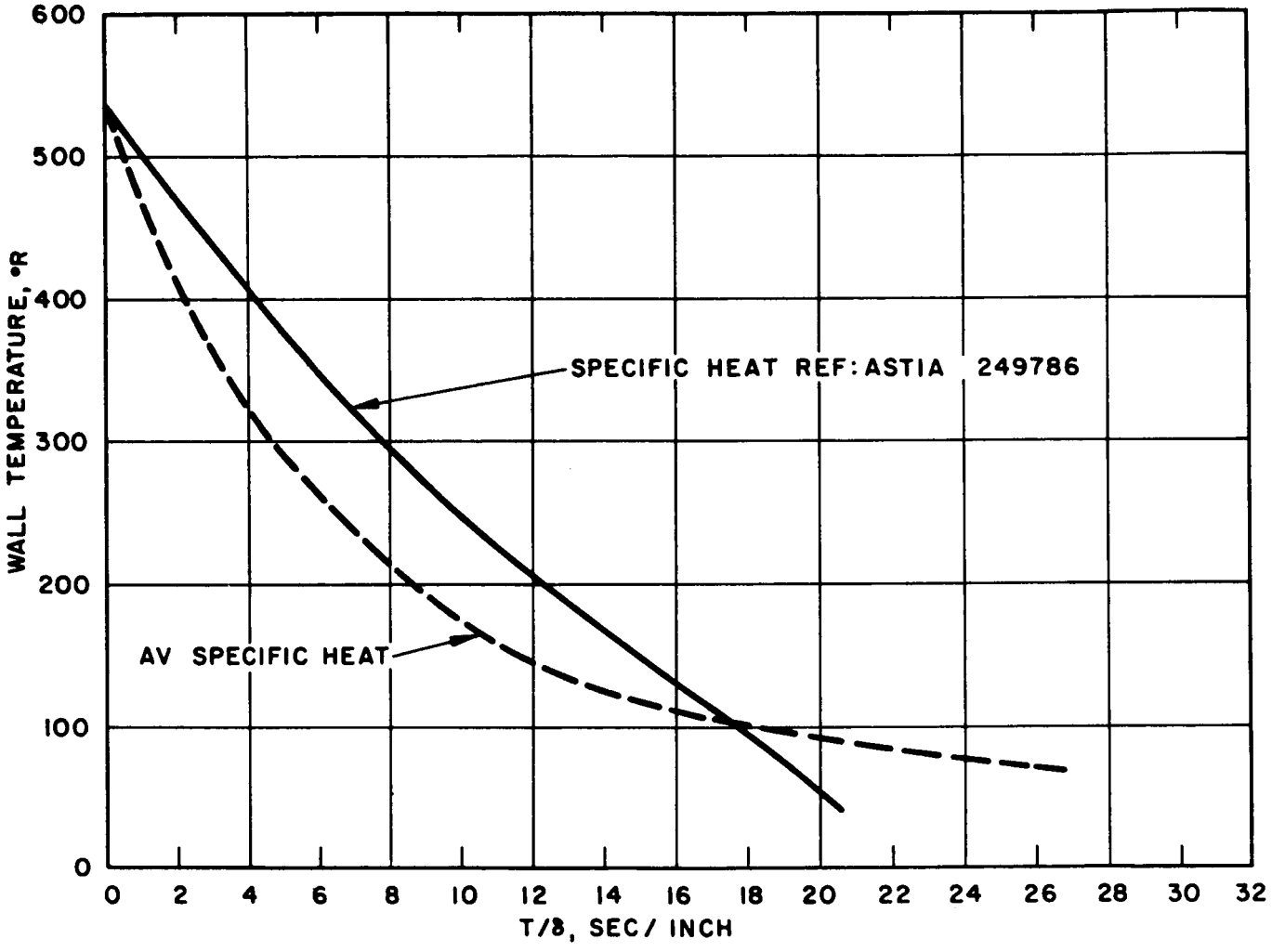

FIGURE 23 - TEMPERATURE HISTORY OF LUMPED PARAMETER SYSTEM ALUMINUM TUBE (θ IN. WALL THICKNESS) 560769

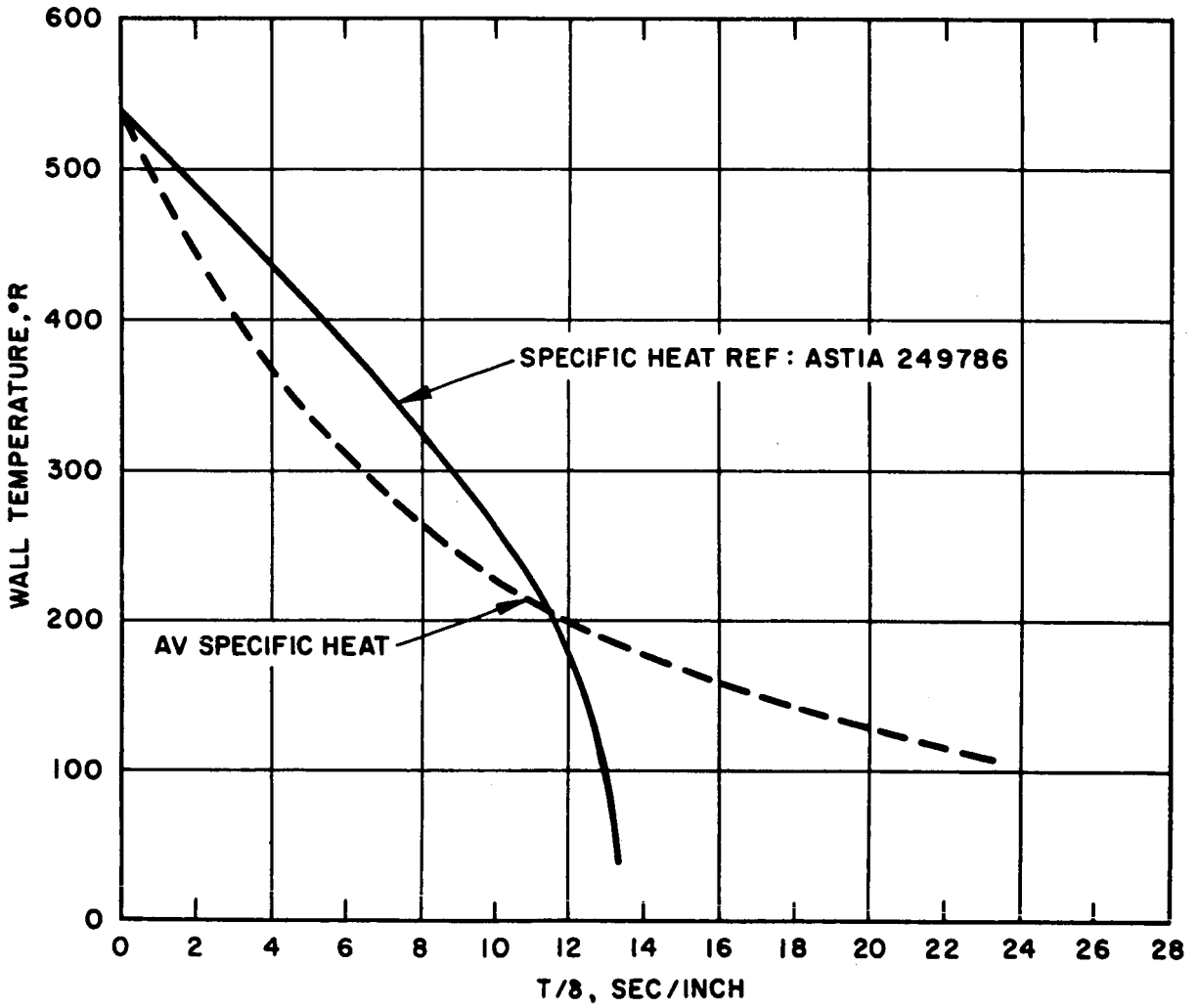

FIGURE 24 - TEMPERATURE HISTORY OF LUMPED PARAMETER SYSTEM BERYLLIUM TUBE (δ INCH WALL THICKNESS)

560770

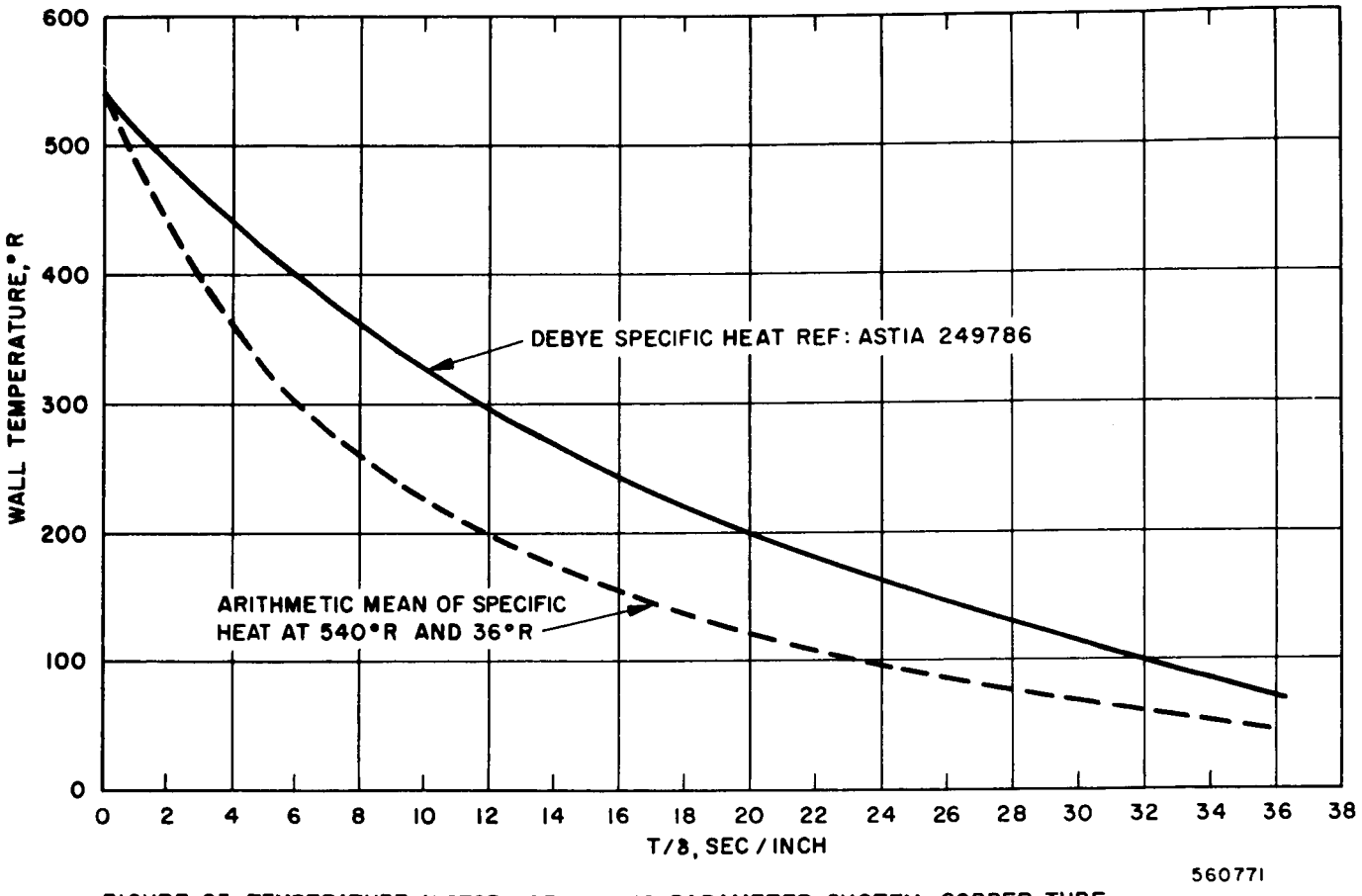

FIGURE 25. TEMPERATURE HISTORY OF LUMPED PARAMETER SYSTEM. COPPER TUBE (δ IN. WALL THICKNESS)